

Phenomenology of the Higgs and Flavour Physics In the Standard Model and Beyond

DISSERTATION

zur Erlangung des akademischen Grades

**doctor rerum naturalium
(Dr. rer. nat.)
im Fach Physik**

**eingereicht an der
Mathematisch-Wissenschaftlichen Fakultät
Humboldt-Universität zu Berlin**

**von
M.Sc. Lina Alasfar
geboren am 27. 09. 1994 in Riad**

**Präsidentin der Humboldt-Universität zu Berlin:
Prof. Dr.-Ing. Dr. Sabine Kunst**

**Dekan der Mathematisch-Wissenschaftlichen Fakultät:
Prof. Dr. Elmar Kulke**

Gutachter:

1. Prof. Dr. R. Gröber, Humboldt-Universität zu Berlin
2. Prof. Dr. Dr. M. Musterman, Potsdam-Institut für Klimafolgenforschung
3. Prof. Dr. M. Mustermann2, Heidelberg

Tag der mündlichen Prüfung: 06. November 2013

Contents

I Higgs Physics	3
1 The Standard Model Higgs boson	5
1.1 Spontaneous symmetry breaking	5
1.1.1 Nambu-Goldstone theorem	8
1.2 The Higgs mechanism	9
1.3 Yukawa interaction	12
1.4 The Higgs and EW precision observables	14
1.4.1 Custodial symmetry	15
1.5 Theoretical constraints on the Higgs	19
1.5.1 Electroweak precision data fits	19
1.5.2 Partial-wave unitarity	19
1.5.3 Other bounds	23
2 Experimental measurements of the Higgs boson	27
2.1 Overview of the Large Hadron Collider	27
2.2 Higgs properties	31
2.2.1 Higgs boson mass measurements	31
2.2.2 Higgs full width	32
2.2.3 Higgs spin and parity	33
2.3 Measurements of Higgs rates and couplings	33
2.3.1 Higgs cross-sections	33
2.3.2 Constraints on Higgs couplings	37
2.3.3 Anomalous couplings	37
2.4 Challenges and outlook	38
3 Higgs and effective field theories	39

List of publications

1. **L. Alasfar**, G. Degrassi, P. P. Giardino, R. Gröber and M. Vitti
Virtual corrections to $gg \rightarrow ZH$ via a transverse momentum expansion
JHEP **05** (2021), 168
arXiv:2103.06225 [hep-ph].
2. **L. Alasfar**, A. Azatov, J. de Blas, A. Paul and M. Valli
B anomalies under the lens of electroweak precision
JHEP **12** (2020), 016
arXiv:2007.04400 [hep-ph].
3. **L. Alasfar**, R. Corral Lopez and R. Gröber
Probing Higgs couplings to light quarks via Higgs pair production
JHEP **11** (2019), 088
arXiv:1909.05279 [hep-ph].

Part I

Higgs Physics

1 The Standard Model Higgs boson

It's very nice to be right sometimes...
it has certainly been a long wait.

Peter Higgs

Write intro here

1.1 Spontaneous symmetry breaking

Before talking about symmetry breaking, we need to discuss the concept of symmetry in physics. Symmetry has an essential role in studying physical systems. It manifests not only as a geometric feature of physical objects but also in the dynamics of physical systems. For example, one can find symmetries in the equation of motion, Lagrangians/Hamiltonians and actions. The magnetisation of materials is a good example of the role that symmetry plays in describing physical behaviour. For instance, **paramagnetic** materials have a positive magnetic susceptibility χ_B due to the random arrangement of their electrons' spins. The paramagnetic material spins arrangement will therefore possess rotational symmetry. The material has no *preferred direction* in space [1]. On the contrary, **ferromagnetic** materials with the electrons' spins aligned in a certain direction, will not have such symmetry as there will be a preferred direction, see Figure 1.1.

In particle physics and quantum field theory, symmetry plays an essential role in the taxonomy and dynamics of elementary particles and their bound states, i.e. hadrons, cf. [2, 3]. There are two types of symmetries considered when studying elementary particles and their quantum fields: external and internal symmetries. The first is the symmetry of the spacetime background. Typically, this is a four-dimensional Poincaré symmetry. However, in some models, higher spacetime dimensions or non-flat geometries are considered. Though there is no current evidence of higher dimensions or indications of non-flat spacetime from colliders and cosmological observations [4]. The second class of symmetries is internal symmetries stemming from the quantum nature of these particles/fields. Because their state is described by a **ray** in complex Hilbert/Fock spaces, internal symmetries are simply symmetries of rotations in these spaces that keep the action variation unchanged. Internal symmetries are usually described in terms of simple

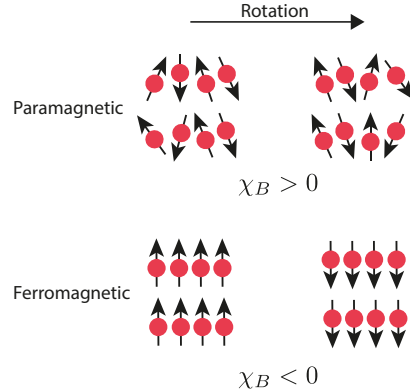


Figure 1.1. In paramagnetic materials, the spins are randomly distributed such that a rotation performed on the system will keep the spin distribution invariant. However, for ferromagnetic materials, where the spins are aligned in a single direction, the symmetry is broken, and the system has a preferred direction.

or product of simple **Lie groups**, e.g. $SU(N)$ ¹, and particles/fields will be arranged as multiplets in some representation of the groups. The rotations of the states could be parametrised by constants. In this case, the symmetry is called **global**, or fields of spacetime, where the symmetry is then called **local** or **gauged**.

Gauge symmetries describe rotations in the state space that depend on spacetime, the generator of the gauge transformations could propagate between two spacetime points. This is the way particle/field interactions are described in quantum field theory. The generators of these gauge transformations are called gauge bosons, and they mediate the interactions between the particles/fields and transform under the adjoint representation of the gauge group. Hence, we observe that gauge symmetries are the basis of describing the fundamental interactions of nature, which we call **gauge theories**.

An example of a gauge theory that is realised in nature is the **Standard Model** (SM). Which is a gauge theory based on the group $G_{\text{SM}} := SU(3)_C \otimes SU(2)_L \otimes U(1)_Y$. The first simple group is for the *strong* interaction described by quantum chromodynamics (QCD). The product of the two remaining groups $SU(2)_L \otimes U(1)_Y$ forms the Weinberg-Salam *electroweak* (EW) model [7–9], where $SU(2)_L$ describes the weak interaction which only couples to *left handed* fermions and $U(1)_Y$ is the weak hypercharge Y gauge group, defined by the formula

$$Y = 2(Q - T_3). \quad (1.1)$$

Where Q is the electric charge and T_3 is the third component of the weak isospin. A description of the matter content of the SM and their multiplicities with respect to G_{SM}

¹Gauge theories based on finite groups have been investigated in the literature, but their phenomenological significance is yet to be further investigated [5, 6]

is shown in Table 1.1

Particle/Field	G_{SM} multiplicity	mass [GeV]
Quarks		
$Q = (u_L^L, d_L^L), (c_L^L, s_L^L), (t_L^L)$	$(\mathbf{3}, \mathbf{2}, 1/6)$	$m_u = 2.16 \cdot 10^{-3}, m_d = 2.67 \cdot 10^{-3}$
$U = u_R, c_R, t_R$	$(\mathbf{3}, \mathbf{1}, 2/3)$	$m_c = 0.93 \cdot 10^{-2}, m_s = 1.27$
$D = d_R, s_R, b_R$	$(\mathbf{3}, \mathbf{1}, -1/3)$	$m_t = 172.4, m_b = 4.18$
Leptons		
$L = (\nu_{e,L}^L, \nu_{\mu,L}^L, \nu_{\tau,L}^L)$	$(\mathbf{1}, \mathbf{2}, -1/2)$	$m_e = 0.511 \cdot 10^{-3}, m_\mu = 1.05 \cdot 10^{-2}$
$E = e_R, \mu_R, \tau_R$	$(\mathbf{1}, \mathbf{1}, -1)$	$m_\tau = 1.77, m_\nu = ??$
Gauge bosons		
$g/G_\mu^A, A = 1 \dots 8$	$(\mathbf{8}, \mathbf{1}, 0)$	0.0
γ/A_μ	$(\mathbf{1}, \mathbf{1}, 0)$	0.0
W_μ^\pm	$(\mathbf{1}, \mathbf{3}, 0)$	80.379
Z_μ	$(\mathbf{1}, \mathbf{3}, 0)$	91.1876
The Higgs boson		
h	$(\mathbf{1}, \mathbf{2}, 1/2)$	125.10

Table 1.1. The SM constituents, their multiplicities with respect to the SM gauge group $G_{\text{SM}} := SU(3)_C \otimes SU(2)_L \otimes U(1)_Y$ and masses. The mass of the neutrinos ν is zero according to the SM prediction, but observations suggest that they are massive, and only the difference between the three masses is known [10]. The values of the masses are taken from the Particle Data Group (PDG) [4], and used throughout this thesis.

The SM has been very successful at describing particle interactions even when challenged by numerous precision tests at LEP and SLD [11–14] and later at DØ [15] and the LHC [16, 17]. Nevertheless, it fails to describe the ground state if only the fermion and gauge sectors are considered. The reason for this shortcoming is that the W^\pm and Z bosons have a mass, this violates the EW gauge symmetry. This can be easily seen by looking at the mass term of a spin 1 field B_μ^A

$$\mathcal{L} = m_B B^{A,\mu} B_\mu^A, \quad (1.2)$$

and performing an $SU(N)$ gauge transformation

$$B_\mu^A \rightarrow B_\mu^A + \partial_\mu \Lambda^A + g \varepsilon_{BC}^A B_\mu^B \Lambda^C. \quad (1.3)$$

We see that the mass term is invariant under these transformations. Secondly, because the SM is a chiral theory, as only left-handed fermions would be doublets under $SU(2)_L$,

the Dirac mass term

$$\mathcal{L}_D = m_D \bar{\psi}_L \psi_R + \text{h.c.}, \quad (1.4)$$

cannot be a singlet under $SU(2)_L$, hence also violating the EW symmetry. Despite quark and lepton masses being forbidden by the EW symmetry, we indeed observe that they do have a mass, and since they also carry charges this mass has to be a Dirac mass.

In order for the EW model to be consistent at the ground state like it is in the interaction states. A mechanism for spontaneous symmetry breaking going from an interaction state to the vacuum ought to be introduced.

1.1.1 Nambu-Goldstone theorem

Coming back to the example of the paramagnetic-ferromagnetic materials, when heated above a certain temperature, known as the **Curie Temperature** T_C will undergo a phase transition and become paramagnetic (losing their permanent magnet property), in the mean-field theory approximation the magnetic susceptibility is related to the temperature of the metal via the relation

$$\chi_B \sim (T - T_C)^{-\gamma}, \quad (1.5)$$

where γ is a critical exponent. We see that if the metal temperature $T > T_C$ the metal is in an *disordered phase* and when $T < T_C$ it is in the *ordered phase*, i.e. χ_B is the **order parameter** of this system. At the Curie temperature, the system will be at the *critical point* where the susceptibility is divergent. The exponent γ is not used to describe the system at the critical point. There is a “pictorial” description of the metal at the critical point which is helpful in picturing the Goldstone theorem. Starting at $T > T_C$, the metal would be in a paramagnetic phase, where the spins are randomly arranged. As the temperature becomes lower and lower, thermal fluctuations start to lessen. One or more regions of the metal, some of the spins will start to get aligned. With continued cooling, nearing T_C , these turned spins will affect their neighbours turning them into their directions. At the critical point $T = T_C$, the system behaves in a peculiar manner, when one would see regions of spins in “up” and others in “down” directions. The system will resemble a fractal of these regions, becoming scale-invariant. Additionally, waves of oscillating local magnetisation will propagate. These waves, or spinless quasiparticles (called **Magnons**) are Goldstone bosons emerging from spontaneous symmetry breaking. Which will manifest at $T < T_C$ as the spins will be arranged in a certain single direction and the metal becomes ferromagnetic.

Theorem 1 (Nambu-Goldstone). When a continuous symmetry has a conserved currents but broken in the ground state (vacuum) is called to be spontaneously broken. There is a scalar boson associated with each broken generator of this spontaneously broken symmetry. The modes of these bosons are fluctuations of the order parameter.

This theorem first emerged from condensed matter physics, particularly superconductors [18, 19]. However, it soon got applied to relativistic quantum field theories [20].

1.2 The Higgs mechanism

In order to solve the aforementioned shortcomings of the Weinberg-Salam model, Nambu-Goldstone theorem has been first proposed by P. W. Anderson [21]. However, the way that Anderson formulated his theory was unfamiliar to particle physicists and used a non-relativistic picture to illustrate how photons could gain mass in an electron plasma with a plasma frequency ω_p

$$m_\gamma^{\text{plasma}} = \frac{\hbar\omega_p}{c^2} \quad (1.6)$$

Later on, a theory that explains the mass generation of the EW gauge bosons has been published in an almost simultaneous manner by R. Braut and F. Englert [22], P. Higgs [23] and G. Guralnik, C. R. Hagen, and T. Kibble [24, 25]². The Higgs mechanism starts by considering the spontaneous symmetry breaking (SSB) of the EW sector of the SM via the pattern

$$SU(2)_L \otimes U(1)_Y \longrightarrow U(1)_Q \quad (1.7)$$

This is achieved by the vacuum expectation value (vev) of a complex scalar field $\phi \sim (\mathbf{1}, \mathbf{2}, +1/2)$, with the Lagrangian

$$\mathcal{L} = D_\mu \phi^* D^\mu \phi - V, \quad V := \mu^2 \phi^* \phi + \lambda(\phi^* \phi)^2, \quad (1.8)$$

with V denoting the Higgs potential, illustrated in Figure 1.2, which gives non-vanishing vacuum for $\mu^2 < 0$. The field ϕ is given explicitly by

$$\phi = \begin{pmatrix} \phi^1 + i\phi^2 \\ \frac{1}{\sqrt{2}}(h + v) - i\phi^3 \end{pmatrix} \quad (1.9)$$

The covariant derivative

$$D_\mu = \partial_\mu - ig_2 \frac{\sigma_a}{2} W_\mu^a - ig_1 \frac{1}{2} B_\mu, \quad (1.10)$$

dictates the coupling between the Higgs field and the EW gauge bosons and g_3 , g_2 and g_1 are, respectively, the coupling constants of $SU(3)_C$, $SU(2)_L$ and $U(1)_Y$. The minimum

²All of these authors have contributed to the theory of SM spontaneous symmetry breaking (SSB). By calling it the “Higgs” mechanism or boson. I, by no means, have intended to ignore the role played by the rest, rather, I wanted to stick the most widely-used terminology in the field.

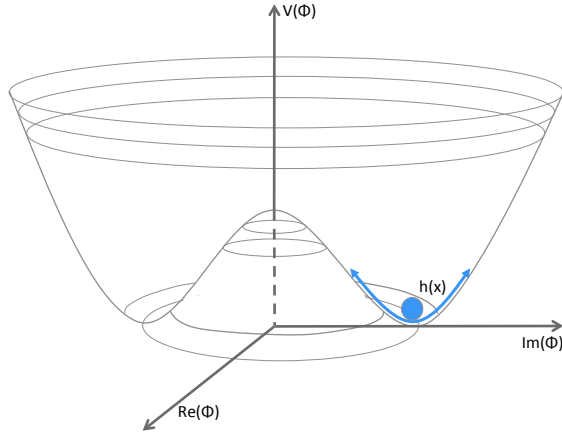


Figure 1.2. The characteristic shape of the Higgs potential showing a non-zero vacuum. While the physical Higgs boson is an oscillation within the energy well illustrated in the diagram with blue arrows., this illustration is taken from [26].

of the scalar potential is then obtained by

$$\frac{\partial V}{\partial \phi} |_{\phi \rightarrow v} = 0, \quad (1.11)$$

which for a tachyonic mass $\mu^2 < 0$ will have a real non-vanishing values v corresponding to the vev of this field $\langle \phi \rangle = (\frac{0}{\sqrt{2}})$.

According to Nambu-Goldstone theorem, the three broken generators of $SU(2)_L \otimes U(1)_Y$ will become massive, and they are the W^\pm and Z bosons, while the photon will remain massless. We will have three massless Goldstone bosons $G^\pm = \frac{1}{2}(\phi^1 \pm i\phi^2)$ and $G^0 = \phi^3$ that are “eaten” by the aforementioned massive photons. Where they become the longitudinal polarisations of W^\pm and Z boson. In order to see this more concretely, we start by looking at the terms of the EW Lagrangian where the field ϕ couples to the gauge bosons, in the unbroken phase

$$D_\mu \phi^* D^\mu \phi = \frac{1}{2} |\partial_\mu \phi|^2 + \frac{1}{8} g_2^2 |\phi|^2 |W_\mu^1 + iW_\mu^2|^2 + \frac{1}{8} |\phi|^2 |g_2 W_\mu^3 - g_1 B_\mu|^2 \quad (1.12)$$

After SSB, we write the gauge bosons in the mass basis

$$\begin{aligned} W_\mu^\pm &= \frac{1}{\sqrt{2}}(W_\mu^1 \pm iW_\mu^2), \\ Z_\mu &= \frac{1}{\sqrt{g_1^2 + g_2^2}}(g_2 W_\mu^3 - g_1 B_\mu), \\ A_\mu &= \frac{1}{\sqrt{g_1^2 + g_2^2}}(g_2 W_\mu^3 + g_1 B_\mu). \end{aligned} \quad (1.13)$$

From this, the electric charge is identified as the coupling constant to the photon A_μ

$$e = \frac{g_1}{\sqrt{g_1^2 + g_2^2}}. \quad (1.14)$$

It is useful to define **Weinberg angle** θ_W , an important EW parameter relating the electric charge to the weak coupling g_2

$$\sin \theta_W = \frac{e}{g_2} \approx 0.231214, \quad (1.15)$$

typically the sin and cos of the Weinberg angle are denoted by s_W and c_W , respectively. We use the unitary gauge, to absorb the Goldstone bosons into the W^\pm and Z longitudinal polarisations. In this gauge the Higgs doublet can be written as

$$\phi \rightarrow \begin{pmatrix} 0 \\ \frac{1}{\sqrt{2}}(h + v). \end{pmatrix}, \quad v = 246 \text{ GeV}. \quad (1.16)$$

With these substitutions, one can read off the masses of the gauge bosons their bilinear terms in (1.12)

$$m_W = \frac{vg_2}{2} \quad m_Z = \frac{v}{2}\sqrt{g_1^2 + g_2^2} \quad m_A = 0. \quad (1.17)$$

Since ϕ is a complex doublet. We have seen that it has four components, and three of them correspond to the Goldstone bosons, thus one remains physical h which is what we now identify with the “Higgs boson” discovered in the Summer of 2012 [27, 28]. The couplings between the Higgs and the electroweak bosons is related to their mass via the vev

$$g_{hVV} = \frac{2m_V^2}{v}, \quad g_{hhVV} = \frac{2m_V^2}{v^2}. \quad (1.18)$$

By substituting (1.16), into the Higgs potential (1.8) one can write the mass of the physical Higgs boson in terms of the vev

$$m_h = \sqrt{2\lambda}v. \quad (1.19)$$

The physical Higgs mass is related to the μ parameter via the relation

$$m_h^2 = -2\mu^2, \quad (1.20)$$

One can see that the mass term after SSB changes its sign, characterising the order-parameter for this system, analogous to the magnetic susceptibility for the magnetisation of materials example. One could also identify the self-couplings of h , the trilinear and quartic couplings

$$g_{hhh} = 3\lambda v = 3\frac{m_h^2}{v}, \quad g_{hhhh} = 3\lambda = 3\frac{m_h^2}{v^2}. \quad (1.21)$$

1.3 Yukawa interaction

It is possible to also use the Higgs vev to give fermions their masses by introducing a Yukawa-interaction terms, first introduced by S. Weinberg [9]

$$\mathcal{L}_{\text{Yuk}} = -y_e \bar{L} \phi E - y_d \bar{Q} \phi D - y_u \bar{Q} \tilde{\phi} U + \text{h.c.}, \quad (1.22)$$

with $\tilde{\phi} = i\sigma_2\phi$ and y_e, y_d, y_u are 3×3 matrices. These matrices are free parameters in the SM. As the Higgs boson acquires a the vev, the fermions will acquire a mass $m_f = vy'_f$ and the Higgs boson coupling to the fermions is given by

$$g_{h\bar{f}f} = \frac{m_f}{v}, \quad (1.23)$$

and the Yukawa matrices will be fixed in the mass basis y'_f by measurements of the fermion masses.

Leptonic Yukawa matrix is diagonal, with a degeneracy between the flavour and masses basis, this manifests as lepton family number conservation (the lepton family operator commutes with the Hamiltonian.). However, for the quarks, the situation is more complicated. One can rotate these matrices to the mass basis via a bi-unitary transformation via the unitary matrices $\mathcal{V}_Q, \mathcal{U}_Q$ for $q = u, d$

$$y_q \longrightarrow y'_f = \mathcal{V}_q^\dagger y_q \mathcal{U}_q = \text{diag}(m_{q_1}, m_{q_2}, m_{q_3}). \quad (1.24)$$

However, there is no degeneracy here as the Hamiltonian does not commute with the quark flavour operator. This is because the transformation matrices for the up and down-type quarks are not the same. The charged EW quark currents contains flavour mixing de-

scribed by the Cabibbo-Kobayashi-Maskawa (CKM) matrix [29, 30]. More details on the flavour sector of the SM is discussed in ??

Figure 1.3 shows all the SM couplings' strengths, with the thickness of the chord is proportional to the strength of the coupling, one can see the Higgs couplings in orange. In

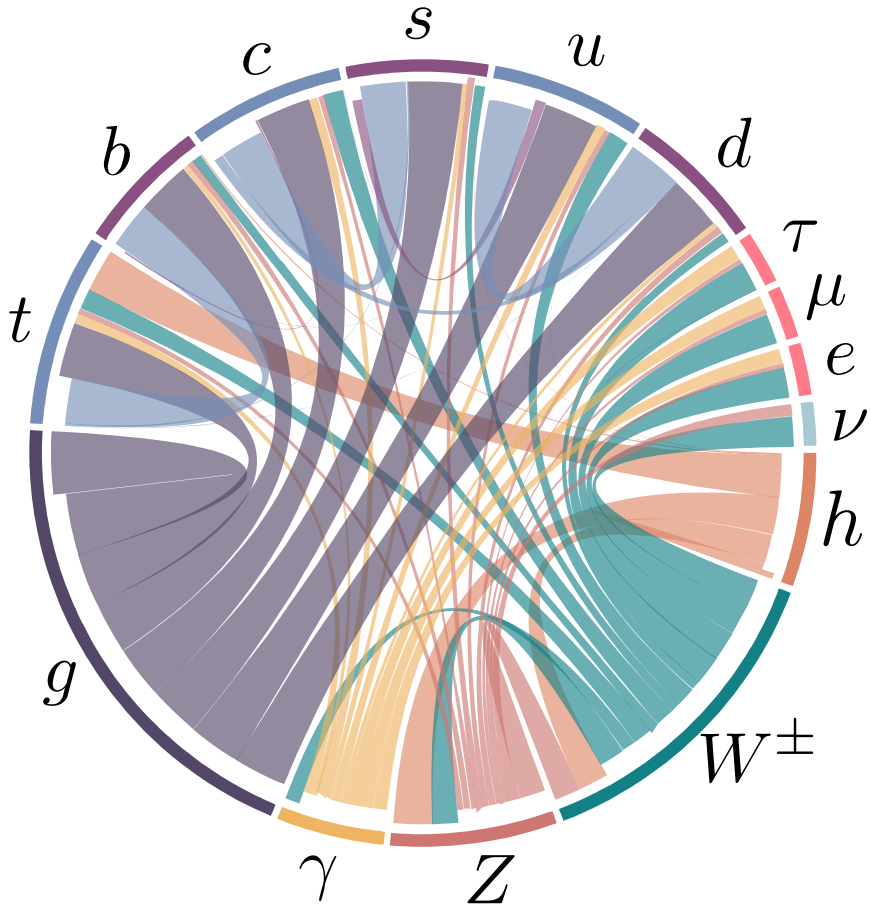


Figure 1.3. The SM Yukawa couplings are proportional to the quark masses, because the Higgs Yukawa couplings span about 6 orders of magnitude, as seen in the case of quarks here. This large hierarchy cannot be explained by the SM.

this figure, we cannot easily see Higgs coupling to the fermions, except for its couplings

to the third generation. Strictly speaking, if we further examined the Yukawa coupling using a logarithmic scale and focused on the quark sector as Figure 1.4 illustrates. We observe that these Yukawa couplings span about 6 orders of magnitudes with marked hierarchy amongst generations. As these couplings are in fact free parameters in the SM, and only determined by the experimental measurements of the quark (or equally applies lepton) masses. This hierarchy of quark masses therefore cannot be explained by the SM Higgs mechanism, and sometimes known as the old flavour puzzle. In later chapters, we will examine the experimental effort to better measure these couplings and how Higgs pair production can be used to probe them in ???. Even the potential of using techniques from *interpretable machine learning* to further improve Higgs pair sensitivity to probing light Yukawas ???. Then in ?? we'll examine the EFT and UV models to modify them.

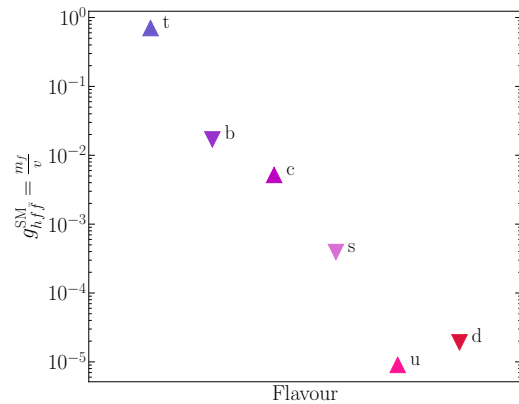


Figure 1.4. A chord diagram showing the SM couplings, with the coupling strength illustrated by the chord thickness. Higgs couplings are coloured in orange.

1.4 The Higgs and EW precision observables

Higgs physics is intertwined with the EW sector for example, the Higgs vev is determined from Fermi's constant $v = (\sqrt{2}G_F)^{-1/2}$, and is fixed by muon lifetime measurements, and comparing it with the theoretical predictions [31–34]

$$\tau_\mu^{-1} = \frac{G_F^2 m_\mu^5}{192\pi^3} \left(1 - \frac{8m_e^2}{m_\mu} \right) \left[1 - 1.810 \frac{\alpha}{\pi} + (6.701 \pm 0.002) \left(\frac{\alpha}{\pi} \right)^2 \right], \quad (1.25)$$

which leads to the numerical value of G_F [4]

$$G_F = 1.1663787(6) \cdot 10^{-5} \text{GeV}^{-2}, \quad (1.26)$$

given the value of the fine structure constant $\alpha^{-1} = 137.03599976(50)$.

Another important EW precision observable (EWPO) is the ratio between the W and Z masses

$$\rho = \frac{m_W^2}{c_W^2 m_Z^2}. \quad (1.27)$$

At leading order, this parameter is equal to unity in the SM. The ρ parameter depends on the representation of the scalar sector of the EW model having ϕ_i scalars with T_i weak isospin and $T_{3,i}$ being its third component, and a vev v_i , via the relation [35, 36]

$$\rho = \frac{\sum_i [T_i(T_i + 1) - T_{3,i}^2] v_i^2}{2 \sum_i T_{3,i}^2 v_i^2}. \quad (1.28)$$

From (1.28) one can see that a real triplet scalar, for instance, would not fit the experimental EW measurement of ρ . Hence, a complex doublet is the simplest scalar possible for the EW symmetry breaking, and the Higgs boson was expected to be seen almost four decades before its discovery. However, radiative corrections to the EW gauge bosons mass from vacuum polarisation diagrams could potentially cause ρ to deviate significantly from unity. This is not the case, as the experimentally measured value of ρ [4]

$$\rho_{\text{exp}} = 1.00038 \pm 0.00020 \quad (1.29)$$

Additionally, it is possible to think of an extended Higgs sector, where there are multiple scalars with different $SU(2)_L$ multiplicities. Or, a composite Higgs sector, where the Higgs boson is a pseudo Nambu-Goldstone boson, cf. [37, 38]. How can such models be built assuring the ρ parameter is protected from change ? The answer to this question lies in a symmetry of the Higgs Lagrangian known as custodial symmetry.

1.4.1 Custodial symmetry

After SSB, a residual global symmetry known as the custodial symmetry protects the ρ parameter from obtaining large radiative corrections at higher orders in perturbation theory. This symmetry must be kept in extended or composite Higgs models. This symmetry can be seen by rewriting the Higgs potential as

$$V = \frac{\lambda}{4} \left(\phi_1^2 + \phi_2^2 + \phi_3^2 + \phi_4^2 - 2\mu^2 \right)^2. \quad (1.30)$$

This potential is invariant under $SO(4) \simeq SU(2)_L \otimes SU(2)_R$ rotations. However, when the Higgs field squires a non-vanishing vev, $\phi_4 \rightarrow h + v$, the potential becomes

$$V = \frac{\lambda}{4} \left(\phi_1^2 + \phi_2^2 + \phi_3^2 + h^2 + 2vh + v^2 - 2\mu^2 \right)^2, \quad (1.31)$$

which is only invariant under $SO(3) \simeq SU(2)_V$ transformations, the diagonal part of the original group. This global SSB pattern comes alongside the EW SSB of the gauge group $SU(2)_L \otimes U(1)_Y$ as global $SU(2)_L$ is itself the gauged $SU(2)_L$ group. Additionally the T^3 component of the $SU(2)_R$ global group is the gauged $U(1)_Y$ and the T^3 component of the custodial group $SU(2)_V$ is gauged as well and identified to be the electric charge operator, i.e. the generator of $U(1)_Q$.

$$\underbrace{SU(2)_R}_{\supset U(1)_Y} \otimes \overbrace{SU(2)_L}^{\text{gauged}} \longrightarrow \underbrace{SU(2)_V}_{\supset U(1)_Q}. \quad (1.32)$$

This pattern indicates that the symmetry is already broken by the gauging of the diagonal part of $SU(2)_R$ (the hypercharge). The custodial symmetry is only *approximate* in the limit of $g_1 \rightarrow 0$, and $\rho = 1$ is a consequence of $g_1 \neq 0$. The symmetry breaking pattern $\mathbf{2} \otimes \mathbf{2} = \mathbf{3} \oplus \mathbf{1}$ also allows us to identify the Goldstone bosons as the custodial triplet and the physical Higgs h as the custodial singlet, explaining the electric charge pattern they have.

We could use the isomorphism between the special orthogonal and special unitary groups to parametrise the Higgs doublet as an $SU(2)_L \otimes SU(2)_R$ bidoublet

$$\mathcal{H} = (\tilde{\phi} \ \phi) = \frac{1}{\sqrt{2}} \begin{pmatrix} \phi_4 - i\phi_3 & \phi_1 + i\phi_2 \\ \phi_1 - i\phi_2 & \phi_4 + i\phi_3 \end{pmatrix}, \quad (1.33)$$

with the bi-unitary transformations

$$\mathcal{H} \longrightarrow \mathcal{U}_L \mathcal{H} \mathcal{U}_R^\dagger \quad (1.34)$$

which leaves any traces of the form $\text{Tr}(\mathcal{H}^\dagger \mathcal{H})$, invariant. The Higgs potential could be rewritten in terms of the bidoublet

$$V = -\frac{\mu^2}{2} \text{Tr}(\mathcal{H}^\dagger \mathcal{H} + \frac{\lambda}{4} (\text{Tr}(\mathcal{H}^\dagger \mathcal{H}))^2) \quad (1.35)$$

The vev is hence written in this representation as

$$\langle \mathcal{H} \rangle = \frac{v}{\sqrt{2}} \mathbb{1}_{2 \times 2}. \quad (1.36)$$

We can also look at the Yukawa sector, and observe that in the case where $y_u = y_d = y$, we can also write the left-handed and right-handed quarks as $SU(2)_L \otimes SU(2)_R$ bidoublets and $SU(2)_R$ doublets, respectively. Hence, the quark part of the Yukawa Lagrangian in (1.22) becomes

$$\mathcal{L}_{yuk} \supset \frac{y}{\sqrt{2}} (\bar{u}_L \ \bar{d}_L) \begin{pmatrix} \phi_4 - i\phi_3 & \phi_1 + i\phi_2 \\ \phi_1 - i\phi_2 & \phi_4 + i\phi_3 \end{pmatrix} \begin{pmatrix} u_R \\ d_R \end{pmatrix}, \quad (1.37)$$

which is invariant under custodial transformations, but when $y_u \neq y_d$, this Lagrangian term breaks custodial symmetry. Thus, the differences between the up-type and down-type quark masses $m_u - m_d$ are considered **spurions** of the custodial symmetry and one expects to see radiative corrections to ρ being proportional to these spurions.

In order to see this more concretely, we start by examining the radiative corrections that could contribute to the deviation of ρ from unity, i.e. $\Delta\rho$ these corrections are known as the **oblique correction**. These oblique corrections come from electroweak vacuum polarisations $\Pi_{VV}(p^2)$, as shown in Figure 1.5, for more details on these corrections and their calculation see Refs.. [39, 40]

The 1-loop correction to the ρ parameter is given in terms of the Π_{VV} by

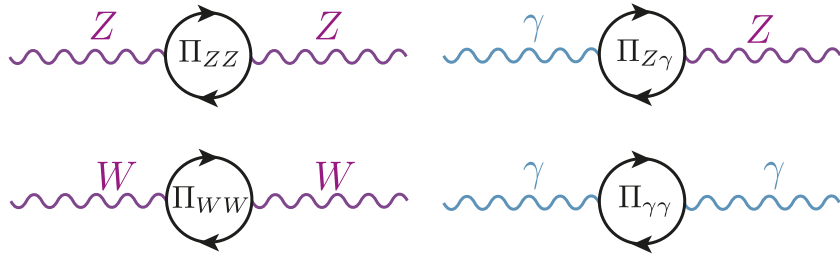


Figure 1.5. The oblique corrections, are radiative correction with electroweak gauge bosons propagators. Namely vacuum polarisations of the Z , W^\pm and γ bosons.

$$\Delta\rho = \frac{\Pi_{WW}(0)}{m_W^2} - \frac{\Pi_{ZZ}(0)}{m_Z^2} \quad (1.38)$$

Where the dominant contributions are given by [41]

$$\Delta\rho = \frac{3G_F}{8\sqrt{2}\pi^2} \left((m_t^2 + m_b^2) - \frac{2m_t^2 m_b^2}{m_t^2 - m_b^2} \ln \frac{m_t^2}{m_b^2} \right) + \dots \quad (1.39)$$

Since $m_b \ll m_t$, the correction is non-vanishing, and (1.39) shows clearly how the radiative corrections are proportional to the spurions of the custodial symmetry. However, this radiative correction is absorbed into the SM definition of ρ , i.e. the $\overline{\text{MS}}$ definition of the ρ -parameter $\rho^{\overline{\text{MS}}}$.

One can study new physics (NP) effects that violates custodial symmetry, by looking at deviations from $\rho = 1$ from it. Given the experimentally measured value of ρ (1.29) many NP models violating custodial symmetry can already be excluded. Nevertheless, ρ alone does not capture the full story of EWPO's. For instance, adding a new quark doublet would not necessarily violate the custodial symmetry though it still can be excluded by EWPO. It is hence useful to introduce new parameters known as **Peskin-Takeuchi parameters** [40, 42, 43]

Peskin-Takeuchi parameters

$$\begin{aligned} S &:= \frac{4c_W^2 s_W^2}{\alpha} \left[\frac{\Pi_{ZZ}^{\text{NP}}(m_Z^2) - \Pi_{ZZ}^{\text{NP}}(0)}{m_Z^2} - \frac{c_W^2 - s_W^2}{c_W s_W} \frac{\Pi_{Z\gamma}^{\text{NP}}(m_Z^2) - \Pi_{\gamma\gamma}^{\text{NP}}(m_Z^2)}{m_Z^2} \right], \\ T &:= \frac{\rho^{\overline{\text{MS}}} - 1}{\alpha} = \frac{1}{\alpha} \left[\frac{\Pi_{WW}^{\text{NP}}(0)}{m_W^2} - \frac{\Pi_{ZZ}^{\text{NP}}(0)}{m_Z^2} \right], \\ U &:= \frac{4s_W^2}{\alpha} \left[\frac{\Pi_{WW}^{\text{NP}}(m_W^2) - \Pi_{WW}^{\text{NP}}(0)}{m_W^2} - \frac{c_W}{s_W} \frac{\Pi_{Z\gamma}^{\text{NP}}(m_Z^2) - \Pi_{\gamma\gamma}^{\text{NP}}(m_Z^2)}{m_Z^2} \right] - S. \end{aligned} \quad (1.40)$$

The NP contributions to the EW vacuum polarisations $\Pi_{VV}^{\text{NP}}(p^2)$ could either come from loop or tree-level effects. Typically both T and U are related to custodial symmetry violation. However, U has an extra suppression factor of m_{NP}^2/m_Z^2 compared to T and S . The most recent fit result for these parameters is [4]

$$\begin{aligned} S &= -0.01 \pm 0.10, \\ T &= 0.03 \pm 0.13, \\ U &:= 0.02 \pm 0.11. \end{aligned} \quad (1.41)$$

But since T and S tend to give stronger constraint on NP, due to the suppression factor of U . One can preform a two-parameter fit of S and T setting $U = 0$, thus shown in Figure 1.6, with the numerical values [4],

$$\begin{aligned} S &= 0.00 \pm 0.07, \\ T &= 0.05 \pm 0.06. \end{aligned} \quad (1.42)$$

The Peskin-Takeuchi parameters are important in constraining effective operators in the Higgs sector , namely

$$\begin{aligned} \hat{O}_S &= \phi^\dagger \sigma_i \phi W_{\mu\nu}^i B^{\mu\nu}, \\ \hat{O}_T &= |\phi^\dagger D_\mu \phi|^2. \end{aligned} \quad (1.43)$$

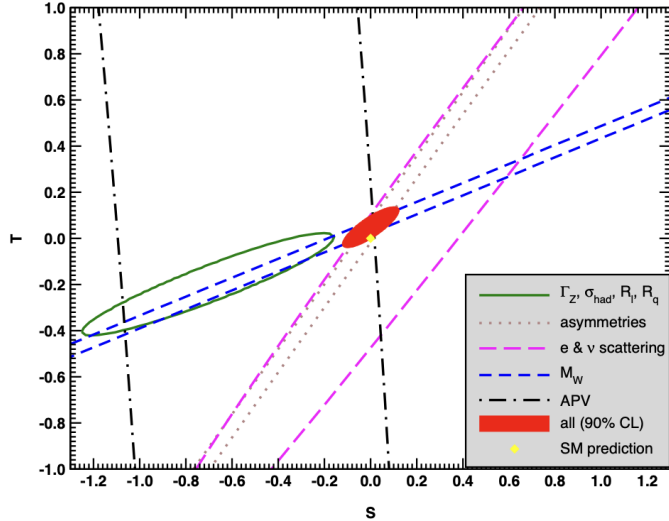


Figure 1.6. Fit results from various EWPO's for T and S setting $U =$. The contours show 1σ contours (39.35% for closed contours and 68% for the rest). This plot is obtained from the PDG [4]

For example, \hat{O}_S appears in Technicolour models causing large deviations of S compared to its measured value [42, 44–46]. Moreover, The constraints on T parameter is important for top mass generation ans well as modifications to $Zb\bar{b}$ coupling in such models [47, 48]. We will revisit the \hat{O}_T when we discuss the Higgs and effective field theories in chapter 3

1.5 Theoretical constraints on the Higgs

1.5.1 Electroweak precision data fits

Even prior to the discovery of the Higgs boson at LHC in 2012, many theoretical aspects of the Higgs sector provided marked bounds on the Higgs properties, particularly its mass. For instance, using the EWPO measurements at LEP provided an input for a fit based of radiative effects coming from the Higgs boson to such observables [11] as in diagram (a) of Figure 1.8, the bounds improved with the improvements of EWPO measurements, these bounds were known as the “blue band” plots seen with their progression in Figure 1.7.

1.5.2 Partial-wave unitarity

. This process Another bound on Higgs mass emerged from studying the amplitudes of EW vector bosons elastic scattering having longitudinal polarisations $V_L V_L \rightarrow V_L V_L$ at high energies $E \gg m_W$ (see diagrams (b) in Figure 1.8), where the Goldstone

equivalence theorem holds [49]. This bound comes from applying the partial wave perturbative unitarity on the EW boson scattering amplitude. I will derive here this bound starting from the **Optical theorem**, which a direct result from the unitarity of the **S** matrix.

The optical theorem

Let \mathcal{M}_{aa} be a covariant matrix element for an elastic scattering process with for a particle a then the following relation applies

$$\sum_f \int d\Phi_n(p_a, p_i^f) |\mathcal{M}_{af}|^2 = 2\Im(\mathcal{M}_{aa}), \quad (1.44)$$

where the sum is over all intermediate states n -particle states f with momenta p_i^f and $d\Phi_n(p_a, p_i^f)$ is the n -particle phase space.

If we only consider a $2 \rightarrow 2$ process with momentum states. $|p_1, p_2\rangle \rightarrow |k_1, k_2\rangle$, then (1.44), after expanding the 2-particle phase space , simplifies to

$$\begin{aligned} & \int \frac{d^3 k_1}{(2\pi)^3 2E_1} \int \frac{d^3 k_2}{(2\pi)^3 2E_2} (2\pi)^4 \delta^4(p_1 + p_2 - k_1 - k_2) |\mathcal{M}(s, t)|^2, \\ &= \frac{1}{16\pi} \int_{-1}^1 d(\cos \theta) |\mathcal{M}(s, t)|^2, \end{aligned} \quad (1.45)$$

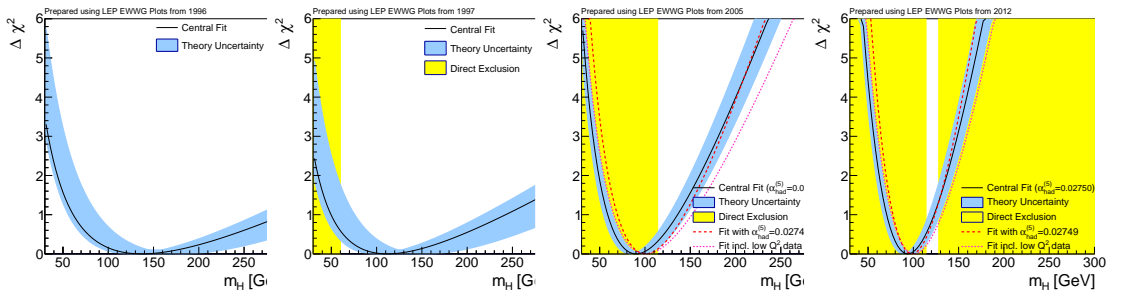


Figure 1.7. Progression of the “blue band” plots with LEP data from 1996 up to 2021 prior to the announcement of the Higgs boson discovery. There plots were taken from [26], based data from LEP [11]

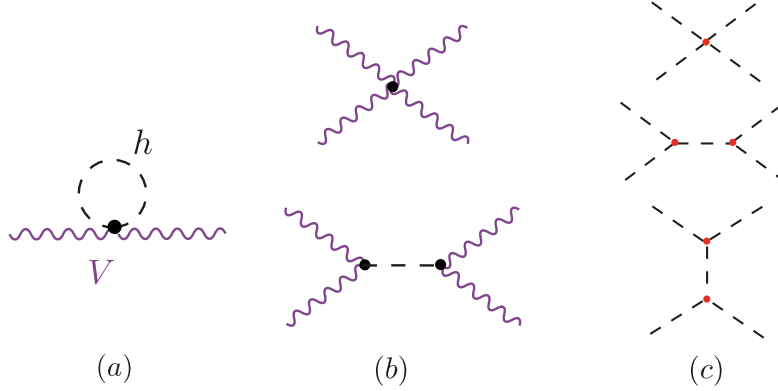


Figure 1.8. Diagrams contributing to theoretical bounds on the Higgs, (a) shows an example of radiative corrections to EWPO from the Higgs bosons. The diagrams in (b) show an elastic scattering of EW vector bosons leading to a bound on the Higgs mass from perturbative unitarity, similarly in (c) diagrams for $hh \rightarrow hh$ scattering leading to constraints on Higgs self-coupling.

with the Mandelstam variables

$$\begin{aligned} s &= k_1 + k_2, \\ t &= k_1 - p_1, \\ u &= k_1 - p_2, \\ s + t + u &= 4m^2 \end{aligned} \tag{1.46}$$

Recall that the relation between the Mandelstam variable t , and the scattering angle for the elastic scattering is given by

$$t = \frac{1}{2}(s - 4m^2)(\cos \theta - 1) \tag{1.47}$$

We could expand the matrix element $\mathcal{M}(s, t)$ in terms of *partial waves*, isolating s from scattering angle dependence

$$\mathcal{M}(s, t) = 16\pi \sum_j (2j+1) a_j P_j(\cos \theta). \tag{1.48}$$

Where a_j are called the j th partial wave amplitude, and $P_j(\cos \theta)$ are the Legendre polynomials

$$P_j(z) = \frac{1}{j!} \frac{1}{2^j} \frac{d^j}{dz^j} (z^2 - 1)^j \tag{1.49}$$

Which satisfies the orthonormality condition

$$\int_{-1}^1 dz P_j(z) P_k(z) = \frac{1}{2j+1} \delta_{jk} \quad (1.50a)$$

$$P_j(1) = 1 \quad \forall j. \quad (1.50b)$$

We hence get for the LHS of (1.44) scattering

$$\begin{aligned} & \int \frac{d^3 k_1}{(2\pi)^3 2E_1} \int \frac{d^3 k_2}{(2\pi)^3 2E_2} (2\pi)^4 \delta^4(p_1 + p_2 - k_1 - k_2) |\mathcal{M}(s, t)|^2, \\ &= \frac{1}{16\pi} \int_{-1}^1 d(\cos \theta) \left[16\pi \sum_j (2j+1) a_j(s) P_j(\cos \theta) \right] \times \\ & \quad \left[16\pi \sum_k (2k+1) a_k^*(s) P_k(\cos \theta) \right], \\ & \Rightarrow = 32\pi \sum_j (2j+1) |a_j(s)|^2. \end{aligned} \quad (1.51)$$

And the RHS of (1.44)

$$2\Im(\mathcal{M}_{aa}) = \underbrace{2\Im(\mathcal{M}(s, 0))}_{t \text{ is integrated out.}} = 32\pi \sum_j (2j+1) \Im(a_j(s)). \quad (1.52)$$

Otherwise large cancellations needed, $a_j(s)$'s are hierarchical. Thus, we could compare the partial wave amplitudes term-by-term

$$|a_j(s)|^2 \leq \Im(a_j(s)) \Rightarrow \Re(a_j(s))^2 + \Im(a_j(s))^2 \leq \Im(a_j(s)) \quad (1.53)$$

Rearranging terms, we get

$$\Re(a_j(s)) + \left(\Im(a_j(s)) - \frac{1}{2} \right)^2 \leq \frac{1}{4} \quad (1.54)$$

The partial wave amplitude has to lie within the unitarity circle. We use though perturbation theory if the partial wave amplitude respects the inequality

$$\Re(a_j(s)) \leq \frac{1}{2} \quad (1.55)$$

This is known as the perturbative partial wave unitarity bound.

When (1.55) is applied for $V_L V_L \rightarrow V_L V_L$, in the Goldstone boson equivalence theorem

regime in particular for $V = W$ boson, we get for the S -wave partial amplitude

$$a_0 \sim \frac{m_h^2}{16\pi v^2} \left(2 + \mathcal{O}\left(m_h^2/s\right) \right). \quad (1.56)$$

Looking at the asymptotic behaviour as $s \rightarrow \infty$, we obtain the bound

$$\frac{m_h^2}{8\pi v^2} < \frac{1}{2} \Leftrightarrow m_h \leq 870 \text{ GeV}. \quad (1.57)$$

Indeed this bound is obsolete now after the Higgs mass measurement, however it is very important to demonstrate the power of this technique in constraining Higgs parameters. As this method can be applied to any elastic scattering with the Higgs acts as a mediator like $ZZ \rightarrow ZZ$, $WW \rightarrow ff$ and constrain the corresponding couplings g_{ZZh} , $g_{f\bar{f}h}$ and so on. An important bound can be derived by examining the Higgs elastic scattering $hh \rightarrow hh$ shown in (c) of Figure 1.8 in order to set bounds on Higgs self-interactions g_{hhh} and g_{hhhh} . This is what exactly has been done in ref. [50] where they have found that the S -wave partial amplitude for this process is given by

$$a_0 = -\frac{1}{2} \frac{\sqrt{s(s-4m_h^2)}}{16\pi s} \left[g_{hhh}^2 \left(\frac{1}{s-m_h^2} - 2 \frac{\log \frac{s-3m_h^2}{m_h^2}}{s-4m_h^2} \right) + g_{hhhh} \right], \quad (1.58)$$

which leads to unitarity bounds on the trilinear g_{hhh} and the quartic g_{hhhh} couplings

$$\left| g_{hhh}/g_{hhh}^{\text{SM}} \right| \lesssim 6.5 \quad \text{and} \quad \left| g_{hhhh}/g_{hhhh}^{\text{SM}} \right| \lesssim 65. \quad (1.59)$$

A stronger constrained can be obtained by looking at the one-loop correction to the $hh \rightarrow hh$ scattering amplitude, within the full kinematic range. The unitarity bound here is obtained by looking at the one-loop amplitude at the threshold, and is given by

$$\left| g_{hhh}/g_{hhh}^{\text{SM}} \right| \lesssim 6. \quad (1.60)$$

These bounds are, hitherto, the strongest on these two couplings even when compared to the ones coming from current experimental searches.

1.5.3 Other bounds

Further theoretical bounds could be obtained by studying quantum effects on the Higgs potential. For example, if we looked at the solution of the renormalisation group equation (RGE) for the Higgs self-coupling λ with the boundary condition $\lambda(v) = \lambda_0$ and

ignoring other SM particle-contributions

$$\lambda(Q^2) = \frac{\lambda_0}{1 - \frac{3}{4\pi^2} \log \frac{Q^2}{v^2}} \quad (1.61)$$

We see that the running of λ will hit a pole, known as **Landau pole** when the denominator vanishes. This will happen at the scale

$$Q_c = v e^{4\pi^2/3\lambda_0} = v e^{4\pi^2 v^2 / 3m_h^2} \quad (1.62)$$

This indicates that the theory will break down at scales larger or equal to Q_c . Since the “critical scale” is a function of the Higgs mass, this allows us to set an upper limit on the Higgs mass assuming the SM will be valid up to a certain scale Q_c . This bound is known as **quantum triviality** bound [51]. This is because the low energy behaviour of (1.61) leads to a vanishing interaction, and if we want the Higgs Lagrangian to be perturbative for all scales, then λ has to be vanishing and the theory becomes non-interacting or *trivial*.

Another bound coming from the RGE of λ is the **stability bound**, which considers the stability of the Higgs potential given the running of λ by requiring that the Higgs potential is an operator bounded from below. This bound is obtained by approximating the solution of the RGE at small λ

$$\lambda(Q^2) \sim \lambda_0 + \frac{1}{16\pi^2} \left[-\frac{12m_t^4}{v^4} + \frac{3}{16} (2g_2^4 + (g_2^2 + g_1^2)^2) \right] \log \frac{Q^2}{v^2} \quad (1.63)$$

For the Higgs potential to be bounded from below $\lambda(Q^2)$ ought to be $\lambda(Q^2) > 0$. With this relation for λ_0 in terms of the mass, we get a bound on m_h

$$m_h^2 > \frac{v^2}{8\pi^2} \left[-\frac{12m_t^4}{v^4} + \frac{3}{16} (2g_2^4 + (g_2^2 + g_1^2)^2) \right] \log \frac{Q^2}{v^2} \quad (1.64)$$

Which leads to $m_h \approx 130$ GeV if we assume that the SM is valid up to the Grand Unified Theory (GUT) scale of $\sim 10^{16}$ GeV and $m_h \approx 180$ GeV for Q being at the Planck scale $\sim 10^{19}$ GeV.

More sophisticated calculations and discussion for the Higgs potential and vacuum stability has been a subject of great interest in pre and post-Higgs discovery eras cf. [51–54] and the most state-of-the-art calculation for the vacuum stability at NNLO has been performed in ref. [55] where they also included finite temperature effects to construct a phase diagram in the $m_t - m_h$ and $m_t - \lambda(M_{pl})$ planes as shown in Figure 1.9. Indicating that the measured Higgs mass is likely compatible with a metastable vacuum rather than absolute stability. This indicates that there is a finite probability for the Higgs vacuum (false vacuum) to decay into a lower energy state (true vacuum) via quantum tunnelling.

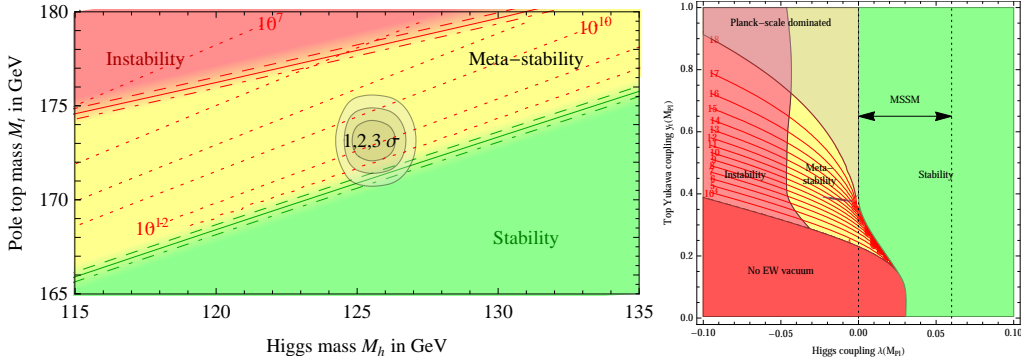


Figure 1.9. Phase diagrams of the Higgs vacuum in the $m_t - m_h$ (left) and $m_t - \lambda(M_{pl})$ (right) planes showing areas of instability, meta stability and absolute stability. In the $m_t - \lambda(M_{pl})$ diagram, the allowed range of the Higgs self-coupling λ in the Minimal Supersymmetric SM (MSSM), this plot is taken from [55]

2 Experimental measurements of the Higgs boson

The observation of the Higgs boson, then the extensive measurement of its properties and couplings has been on the top of the LHC programme priorities [56]. In the time this thesis was in the writing, the particle physics community will be celebrating a decade since the Higgs boson's discovery. Looking back 10 years ago, when I have witnessed the discovery of the Higgs boson via news press-conference in summer of 2012, and decided to be a part of this enormous step that humanity has taken, I feel astonished by the progress made in understanding this newly discovered particle!

In this chapter, I will start by an overview of the extraordinary LHC and its experiments in section 2.1. Then, I will review the state-of-the-art status of experimental measurements of the Higgs properties in section 2.2, cross-sections and couplings in section 2.3, and at the end I will discuss the challenges and outlook for the future runs of the LHC section 2.4, of which the rest of this thesis is going to be aimed to address a small part of them.

2.1 Overview of the Large Hadron Collider

The Large Hadron Collider (LHC) is the largest particle accelerator in the CERN accelerators complex, with a circumference of about 26 km, with over 9590 superconducting magnets cooled to 1.9 K. It was built as an upgrade to the Large electron positron collider (LEP) which ended its operation in the year 2000. The LHC contains four main experiments situated at the four beam collision points and detectors, and these experiments are: ATLAS, CMS, LHCb and ALICE, there also smaller experiments such as LHCf, MilliQan, TOTEM and others. For more details about the LHC cf. [57, 58] or see the LHC technical design report [59] for more technical details.

The LHC started operation in September of 2008, with low energy proton beams, then gradually increased to an energy of 3.5 TeV per proton to reach a centre of mass energy \sqrt{s} of 7 TeV, and data-taking period started from 2011. By 2012, its energy has increased to $\sqrt{s} = 8$ TeV and operated at this energy for about a year and half, then stopping in mid 2013 concluding what is known as **Run-I**. In 2015, the **Run-II** started with almost double the energy $\sqrt{s} = 13$ TeV, and lasted for ca. 3 years. As this thesis being written, preparations are being made to get **Run-III** started until 2024. During these runs, heavier nuclei such as ^{207}Pb and ^{131}Xe have been collided either with protons or

with themselves [60].

From, 2025 and beyond, the **High-Luminosity** LHC (HL-LHC) era will commence, see [Figure 2.2](#). Where the LHC will be shutdown for extensive upgrades [61] to potentially increase its energy to $\sqrt{s} = 14$ TeV and higher collision rates hence the term *high luminosity*. Which leads us to an important notion in particle physics phenomenology *integrated luminosity*.

The performance of colliders depends on many factors, but for phenomenological studies, like this thesis, one mainly considers the centre of mass energy \sqrt{s} and the integrated luminosity \mathcal{L} . This is mainly due to the fact that particle colliders experiments are basically “counting experiments”, and all of the bounds on physical observables or model parameters are obtained from the number of signal versus background events, and the number of expected events $N_{\text{exp}}^{\text{spec}}$ for a given resonance R and a subsequent decay final state X at any collider experiments is given by

$$N_{\text{exp}}^{\text{spec}} = \sigma(pp \rightarrow R) \mathcal{B}(R \rightarrow X) \mathcal{L} \epsilon_{\text{SEL}}. \quad (2.1)$$

Here ϵ_{SEL} is the selection efficiency, which depends on many factors like the detector geometry and particle identification performance etc., as well as the signal one searches for, it can be improved by better detected or selection cuts. The production cross-section increases typically with quadratically with \sqrt{s} , hence comes the need for higher energies but this can only achieved by building new colliders from scratch. The integrated luminosity can be increased much more easily, by longer running time of the same collider as it is the time integral of the collider’s luminosity $L(t)$ over its operation time T

$$\mathcal{L} = \int_0^T L(t) dt. \quad (2.2)$$

Therefore, we see that the integrated luminosity for the LHC experiments will increase over time, when more collisions taking place, as seen in figure [Figure 2.1](#) showing the integrated luminosity for ATLAS and CMS experiments. As the protons travel in the LHC in **bunches**, and as these bunches cross, protons collide at a certain frequency f , when two bunches with N_1 and N_2 protons per bunch, respectively. Each bunch will have an effective cross-section $4\pi\sigma_i$ corresponding to their physical sizes $\sigma \sim 16 \mu\text{m}$, the luminosity is therefore given -approximately- by

$$L = \frac{f N_1 N_2}{4\pi\sigma_1\sigma_2}, \quad (2.3)$$

which is for the LHC averages to about 10^{34} collisions $\text{cm}^{-2}\text{s}^{-1}$ [62, 63].

The total physics-viable pp -collisions integrated luminosity for Run-I was 4.57 /fb for 7 TeV and 20.3 /fb for 8 TeV (ATLAS [64]) and 5.55 /fb at 7 TeV and 21.8 /fb at 8 TeV

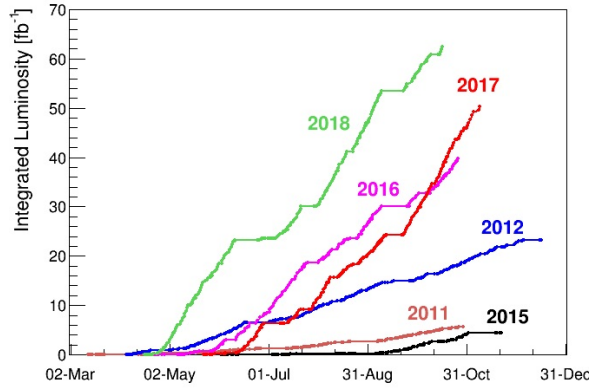


Figure 2.1. The integrated luminosity of the CMS and ATLAS experiments combined over the period from 2011-2018, source [62].

(CMS [65]). As for Run-II the integrated luminosity is 139 /fb at 13 TeV (ATLAS [66]) and 137 /fb at 13 TeV (CMS [65]). The expected integrated luminosity by the end of Run-III is 300 /fb [67] and 3000 /fb by the end of the HL-LHC at energy of 14 TeV [61].



Figure 2.2. A timeline of the LHC operation showing Run-I, Run-II and future planned runs of the LHC, including the HL-LHC, source [60].

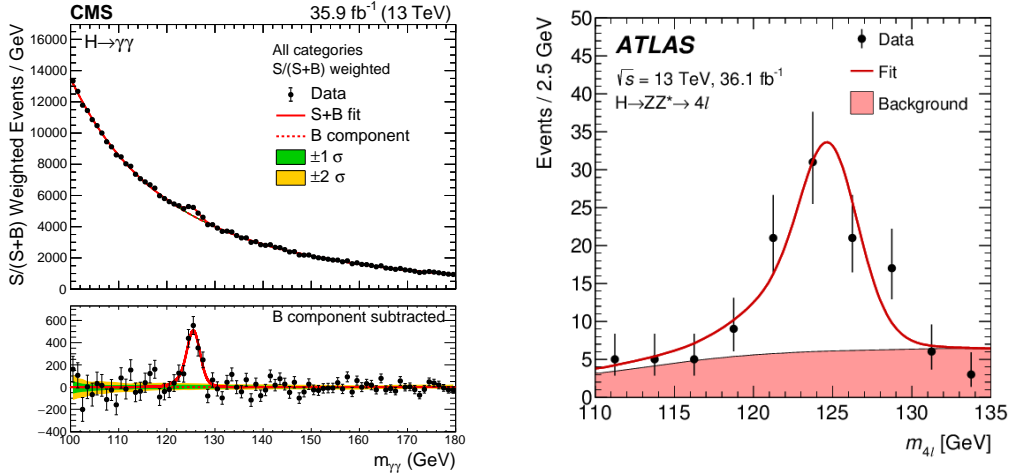


Figure 2.3. The invariant mass distributions of diphoton $m_{\gamma\gamma}$ (CMS [68]) and four lepton $m_{4\ell}$ (ATLAS [69]) final states showing a clear peak at the Higgs mass, with smooth background. These final states are ideal for Higgs mass measurements.

2.2 Higgs properties

2.2.1 Higgs boson mass measurements

In order to measure the mass of the Higgs boson with high precision, one needs to consider final states that can be reconstructed with high momentum and mass resolution, this is typically achieved when no hadronic constituents in the decays involved, such as $h \rightarrow \gamma\gamma$ and $h \rightarrow ZZ^* \rightarrow 4\ell$. Reconstructing the invariant mass distributions $m_{\gamma\gamma}$ and $m_{4\ell}$ one observes that the Higgs peak is narrow over a relatively smooth background, see Figure 2.3, which is ideal for the measurement of the Higgs mass. It should be noted that the width of the resonance is due to the detector resolution and does not correspond to the actual Higgs width.

There have been consistent improvements of the Higgs mass measurements since its discovery. In Figure 2.4 I have performed a meta analysis on ATLAS and CMS measurements of the Higgs mass in Run-I and Run-II of the LHC for both diphoton and ZZ^* final states based on the data from the studies [68–71] using a random effects model [72]. The pooling of the studies yielded a mass measurement of $m_h = 125.21 \pm 0.10$, which translates to a 0.11% accuracy, the heterogeneity of the studies was found to be $I^2 = 49\%$ ($p = 0.05$). Different measurements combination techniques were used in [68] and [4] yielded different central values but all of the results agree within the uncertainties.

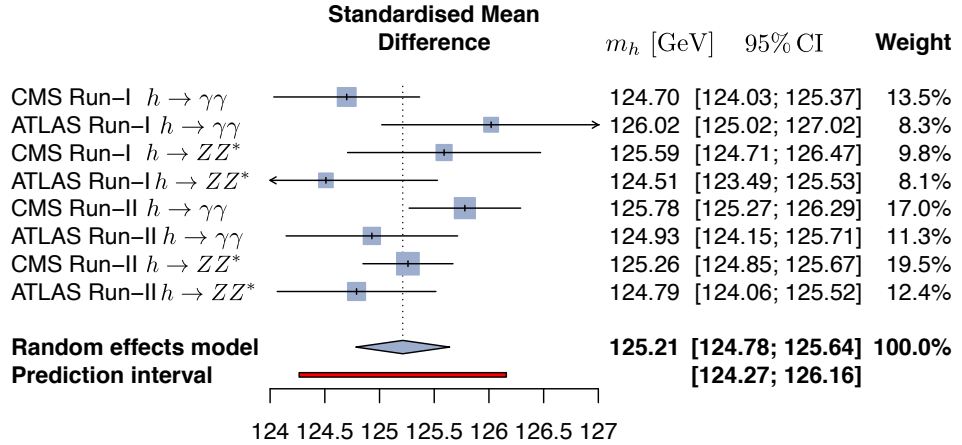


Figure 2.4. A meta analysis preformed to combine all the measurements of the Higgs mass from Run-I and Run-II, the combined result was obtained from pooling all of the studies using the random effects model method.

2.2.2 Higgs full width

The SM values of the Higgs boson full width is $\Gamma_h = 4.1$ GeV and it can be accessed in the LHC by looking at the ratio of on-shell versus off-shell Higgs production and decay to the $ZZ^{(*)}$ state, and $ZZ^{(*)} \rightarrow 4\ell, 2\ell 2\nu$, namely

$$\frac{\sigma(gg \rightarrow h \rightarrow ZZ^*)}{\sigma(gg \rightarrow h^* \rightarrow ZZ)} = \kappa_g^2 \kappa_Z^2 \frac{4m_Z^2}{m_h \Gamma_h}, \quad (2.4)$$

where the κ here denote the ratio between the measured/ or modified coupling with the Higgs and the SM prediction, i.e.

$$\kappa_X := \frac{g_{XXh}}{g_{XXh}^{\text{SM}}}. \quad (2.5)$$

Which is commonly used in reporting experimental constrains/ measurements of the Higgs couplings, as in the next section [section 2.3](#). We shall discuss the κ formalism more in [chapter 3](#).

We see from (2.4) that if one fixes the coupling between the gluons and the Z boson and the Higgs it is possible to access the full width directly. Unfortunately, it is not possible to directly measure the Higgs full width at the LHC, as this requires full reconstruction of the collision event and study the recoil mass which is only possible at lepton colliders [73, 74]. Alas, it is still possible to extract bounds on Γ_h using (2.4). ATLAS used this method to constrain the full width of the Higgs using Run-II data [75], while CMS has performed the same analysis using Run-I and Run-II data combined [76], the results are 95% CL bounds of Γ_h

$$\Gamma_h < 14.4 \text{ GeV} \quad (\text{ATLAS}) \quad 0.08 \text{ GeV} < \Gamma_h < 9.16 \text{ GeV} \quad (\text{CMS}), \quad (2.6)$$

with the combined bound being $\sim 3\Gamma_h^{\text{SM}}$.

2.2.3 Higgs spin and parity

As we have seen in [section 1.2](#), the Higgs boson is a scalar and \mathcal{CP} even ($J^p = 0^+$) in the SM. However, the discovery of a peak in the $m_{\gamma\gamma}$ distribution, would not automatically imply that the particle discovered is scalar, it could be a spin-2 boson, or a pseudoscalar ($J^p = 0^-$). In order to study the J^p properties of the Higgs, one needs to examine the differential distributions of angular variables such as rapidity y or transverse momentum p_T . Both ATLAS and CMS collaborations studied using Run-I data the angular distributions of the Higgs decays $h \rightarrow ZZ^*$, $h \rightarrow WW^*$ and $h \rightarrow \gamma\gamma$. Then test the alternative hypothesis for J^p against the SM [77, 78]. As seen in [Figure 2.5](#), showing CMS results, that the SM 0^+ hypothesis is favoured at $> 99.9\%$ CL.

2.3 Measurements of Higgs rates and couplings

2.3.1 Higgs cross-sections

The total inclusive Higgs cross-section has been measured using the final states $h \rightarrow \gamma\gamma$ and $h \rightarrow ZZ^* \rightarrow 4\ell$. and their combinations. The measurements have been done at the three energies the LHC was operating at: 7 TeV, 8 TeV [79] and 13 TeV [80–82] and combined with more data and compared to the SM prediction as shown in [83]. As shown in [Figure 2.6](#), the measured inclusive cross-section is in agreement with the SM prediction across all of the LHC operation energies.

In addition to the inclusive cross-section measurements, differential cross-sections of the Higgs have been measured for p_T and y as we have seen in [subsection 2.2.3](#) for Higgs's J^p determination. Additional, the differential cross-sections for other variables have

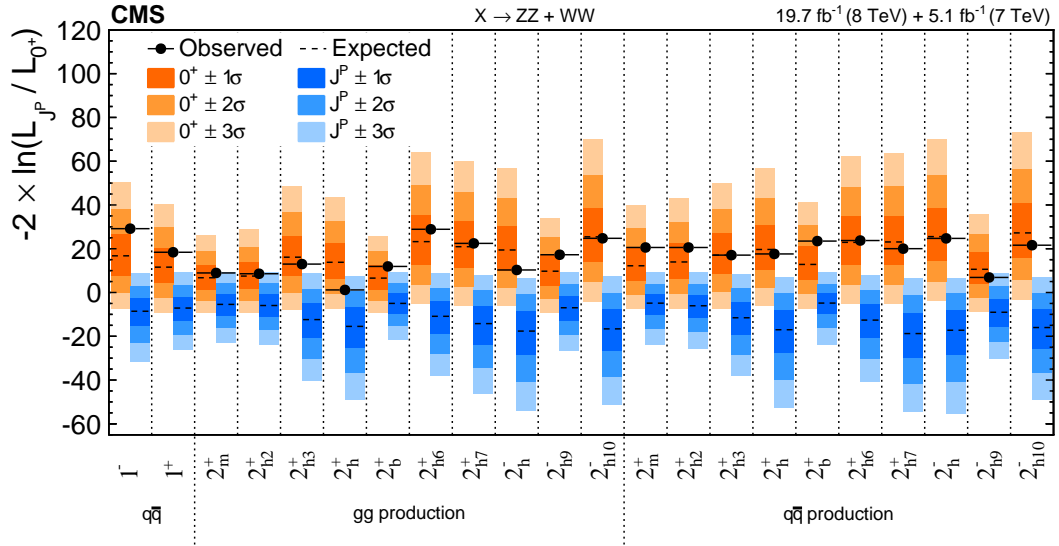


Figure 2.5. The test-statistic distributions for the SM Higgs hypothesis versus other J^P hypotheses in the x axis. The hypothesis testing was conducted using the $h \rightarrow ZZ^*$, $h \rightarrow WW^*$ final-states. The SM hypothesis is indicated in orange, while the alternatives are in blue. Measurements are indicated in black points. This plot is from the CMS collaboration [78]

been measured, and they include $N_{jets}, p_T^{jet}, m_{jj}, \delta\phi_{jj}$ and others using the channels $h \rightarrow ZZ^*$, $h \rightarrow WW^*$ and $h \rightarrow \gamma$. The most recent results using the full Run-II data can be found in Refs. [81, 83–85].

In addition to the total inclusive cross-section, a collection of measurements of Higgs production and decay rates has been carried out by both ATLAS and CMS. These measurements also carried out in , what is known as Standard Template Cross-Sections (STXS) framework. The STXS's are fiducial cross-sections in exclusive phase-space regions or bins separately per Higgs boson production channel. They have the advantage of standardisation of cuts and final results such that measurements could be easily combined across analyses. More details about the STXS framework can be found in the reports of LHC Higgs cross-sections working group (LHCHXSWG) cf. [86]. In Table 2.1 I summarise the state-of-art measurements of the Higgs rates separated into production and decay channels using the total LHC Run-II data from ATLAS and CMS experiments. Additionally, I give the HL-LHC projections from CMS experiment as a comparison. The results in this table are written in terms of the signal strength, which is directly extracted from measuring the number of events dividing them by the standard model,

$$\mu_{\text{Exp}} := \frac{\sigma \cdot \mathcal{B}}{\sigma^{\text{SM}} \cdot \mathcal{B}^{\text{SM}}} \quad (2.7)$$

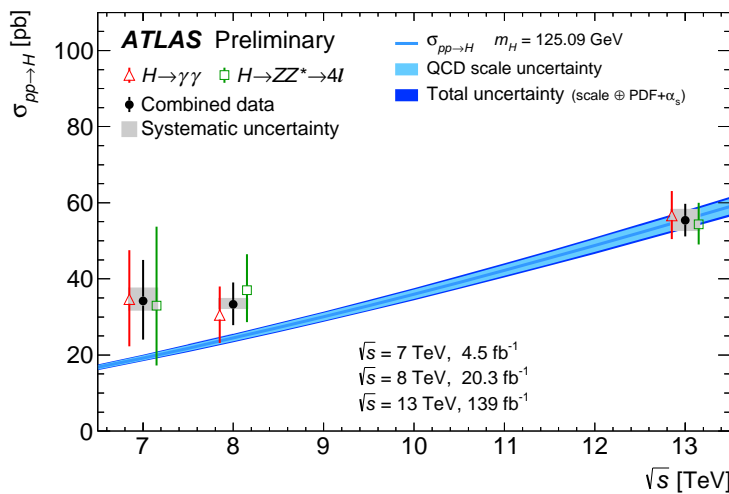


Figure 2.6. The total inclusive cross-section measurements by ATLAS collaboration [83] for 7, 8 and 13 TeV using $h \rightarrow \gamma\gamma$ and $h \rightarrow ZZ^* \rightarrow 4\ell$. channels and their combination (black points) compared to the SM prediction with the uncertainties shown as blue line with light and dark blue bands for QCD scale uncertainties and total uncertainties, respectively.

2 *Experimental measurements of the Higgs boson*

Production	Decay	$\mu_{\text{Exp}} \pm \delta\mu_{\text{Exp}}$ (symmetrised)		Ref.	
		LHC Run-II			
		CMS 137 fb^{-1}	ATLAS 139 fb^{-1}		
ggF	$h \rightarrow \gamma\gamma$	0.99 ± 0.12 1.030 ± 0.110		1.000 ± 0.042 [87–89]	
	$h \rightarrow ZZ^*$	0.985 ± 0.115 0.945 ± 0.105		1.000 ± 0.040	
	$h \rightarrow WW^*$	1.285 ± 0.195 1.085 ± 0.185		1.000 ± 0.037 [87, 89, 90]	
	$h \rightarrow \tau^+\tau^-$	0.385 ± 0.385 1.045 ± 0.575		1.000 ± 0.055	
	$h \rightarrow b\bar{b}$	2.54 ± 2.44 —		1.000 ± 0.247 [89, 90]	
	$h \rightarrow \mu^+\mu^-$	0.315 ± 1.815 —		1.000 ± 0.138 [89, 90]	
VBF	$h \rightarrow \gamma\gamma$	1.175 ± 0.335 1.325 ± 0.245		1.000 ± 0.128 [87–89]	
	$h \rightarrow ZZ^*$	0.62 ± 0.41 1.295 ± 0.455		1.000 ± 0.134	
	$h \rightarrow WW^*$	0.65 ± 0.63 0.61 ± 0.35		1.000 ± 0.073 [87, 89, 90]	
	$h \rightarrow \tau^+\tau^-$	1.055 ± 0.295 1.17 ± 0.55		1.000 ± 0.044	
	$h \rightarrow b\bar{b}$	3.055 ± 1.645 —		— [87]	
	$h \rightarrow \mu^+\mu^-$	3.325 ± 8.075 —		1.000 ± 0.540 [89]	
$t\bar{t}h$	$h \rightarrow \gamma\gamma$	1.43 ± 0.30 0.915 ± 0.255		1.000 ± 0.094 [87–89]	
	$h \rightarrow VV^*$	$0.64 \pm 0.64 (ZZ^*)$ $0.945 \pm 0.465 (WW^*)$ 1.735 ± 0.545	$1.000 \pm 0.246 (ZZ^*)$ $1.000 \pm 0.097 (WW^*)$ —		
	$h \rightarrow \tau^+\tau^-$	0.845 ± 0.705 1.27 ± 1.0	1.000 ± 0.149	[87, 89, 90]	
	$h \rightarrow b\bar{b}$	1.145 ± 0.315 0.795 ± 0.595	1.000 ± 0.116		
	$h \rightarrow \gamma\gamma$	0.725 ± 0.295 1.335 ± 0.315	$1.000 \pm 0.233 (Zh)$ $1.000 \pm 0.139 (W^\pm h)$	[87–89]	
	$h \rightarrow ZZ^*$	1.21 ± 0.85 1.635 ± 1.025	$1.000 \pm 0.786 (Zh)$ $1.000 \pm 0.478 (W^\pm h)$	[87, 89, 90]	
Vh	$h \rightarrow WW^*$	1.850 ± 0.438 —	$1.000 \pm 0.184 (Zh)$ $1.000 \pm 0.138 (W^\pm h)$	[89, 91]	
	$h \rightarrow b\bar{b}$	$—$ 1.025 ± 0.175	$1.000 \pm 0.065 (Zh)$ $1.000 \pm 0.094 (W^\pm h)$	[87, 89]	
	Zh CMS	$h \rightarrow \tau^+\tau^-$ $h \rightarrow b\bar{b}$	1.645 ± 1.485 0.94 ± 0.32	— [90]	
	$W^\pm h$ CMS	$h \rightarrow \tau^+\tau^-$ $h \rightarrow b\bar{b}$	3.08 ± 1.58 1.28 ± 0.41		

Table 2.1. The experimental single Higgs production and decay rates measurements from the complete data of LHC Run II and projections for the HL-LHC. The uncertainties were symmetrised here.

2.3.2 Constraints on Higgs couplings

The measurements of the Higgs rates and their combination (also including STXS) have been used to set bounds on the Higgs couplings, the most recent bounds - as this thesis being written - have been reported by ATLAS using the Higgs inclusive rates and STXS for the full Run-II data [92], and by CMS using Higgs rates shown in Table 2.1 [90]. In Figure 2.7, I present the aggregation the ATLAS and CMS bounds on the Higgs coupling modifiers in the κ formalism defined in eq. (2.5). The aggregation of these bounds was preformed using the method described in [93] assuming there is no correlation between ATLAS and CMS measurements.

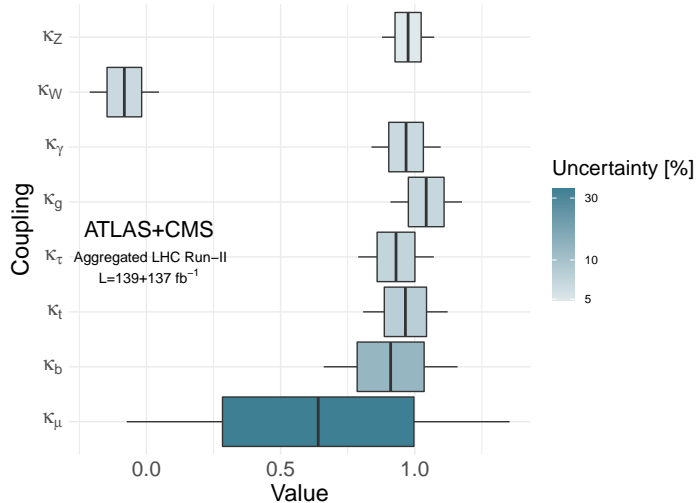


Figure 2.7. Meta analysis aggravating the most recent bounds from ATLAS [92] and CMS [90] on the Higgs coupling modifiers κ .

Examining Figure 2.7, we observe that the bounds on the Higgs boson's coupling to the gauge boson, including the effective couplings to γ and g , as well as the couplings to the third-generation fermions are in few percent within the SM prediction. The bounds on the coupling to the W seems to favour a negative value in CMS fits, due to the channel used to constraint it $h \rightarrow WW$ which depends on κ_W^2 , thus making the best fit value of ~ -1 within the SM prediction. An independent analysis on the relative signs of κ_W and κ_t was preformed using th process in Ref. [94]

2.3.3 Anomalous couplings

to measure HVV CMS used the same data for extraction of the Γ_h to study this [76]

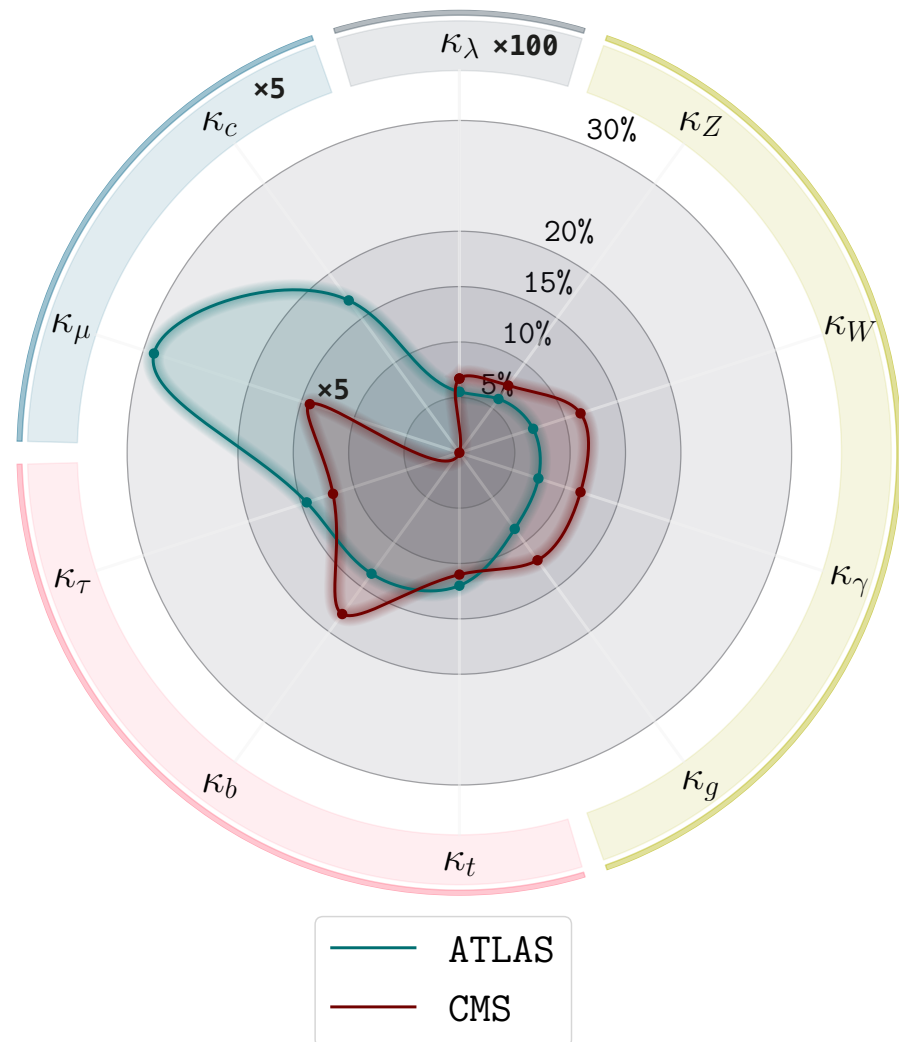


Figure 2.8. ddd

2.4 Challenges and outlook

3 Higgs and effective field theories

If the new BSM degrees of freedom are much heavier than the electroweak scale, a general description of potential new physics effects can be formulated in the language of an effective field theory (EFT). One possibility of such a parameterization is the so-called Standard Model EFT (SMEFT), in which new physics effects are given in terms of higher-dimensional operators involving only SM fields and that also respect the SM gauge symmetries. The dominant effects on Higgs physics, electroweak physics and top quark physics stem from dimension-six operators, suppressed by the new physics scale Λ . This approach is justified in the limit in which energy scales $E \ll \Lambda$ are probed.

In the presence of a gap between the electroweak scale and the scale of new physics, Λ , the effect of new particles below the new physics scale can be described by an EFT. In the case of the SMEFT, the SM Lagrangian is extended by a tower of higher-dimensional operators, \mathcal{O}_i , built using the SM symmetries and fields (with the Higgs field belonging to an $SU(2)_L$ doublet), and whose interaction strength is controlled by Wilson coefficients, C_i , suppressed by the corresponding inverse power of Λ . In a theory where baryon and lepton number are preserved, the leading order (LO) new physics effects are described by the dimension-six SMEFT Lagrangian,

$$\mathcal{L}_{\text{SMEFT}}^{d=6} = \mathcal{L}_{\text{SM}} + \frac{1}{\Lambda^2} \sum_i C_i \mathcal{O}_i. \quad (3.1)$$

A complete basis of independent dimension-six operators was presented for the first time in [95], the so-called *Warsaw basis*.

This note aims at summarising the ongoing efforts for EFT tools for HH and intends to give recommendations for the use of various EFT parameterisations for HH . The note will map the current efforts and outlines where further efforts are needed.

We distinguish between two different kind of EFTs with different assumptions made on the Higgs field, SM effective field theory (SMEFT) and Higgs effective field theory (HEFT), the latter is also referred to as non-linear chiral electroweak Lagrangian. In SM effective field theory the Higgs boson is assumed to transform as in the SM as a $SU(2)$ doublet. The effective Lagrangian the allows for all operators compatible with the symmetries of the SM. For the Higgs boson sector, the leading operators arise at the

dimension-6 level. We define the SM Lagrangian as

$$\begin{aligned}\mathcal{L} = & (D_\mu \phi)^\dagger (D^\mu \phi) - \mu^2 |\phi|^2 - \lambda |\phi|^4 - \left(y_d \bar{q}_L \phi d_R + y_u \epsilon_{ab} \bar{q}_{La} \phi_b^\dagger u_R + \text{h.c.} \right) \\ & - \frac{1}{4} B_{\mu\nu} B^{\mu\nu} - \frac{1}{4} W_{\mu\nu}^a W^{\mu\nu,a} - \frac{1}{4} G_{\mu\nu}^a G^{\mu\nu,a} + \sum_{\psi=q,u,d,\ell} \bar{\psi} \not{D} \psi\end{aligned}\quad (3.2)$$

A summation over the different generations of quarks (q , u and d) and leptons (ℓ) is assumed implicitly. The $SU(2)_L$ doublet field in the unitary gauge is given by $\phi = 1/\sqrt{2}(0, v + h)^T$ with v denoting the vacuum expectation value, $v \approx 246$ GeV. The covariant derivative is defined as conventionally with the plus sign and $G_{\mu\nu}$, $W_{\mu\nu}$ and $B_{\mu\nu}$ are the $SU(3)$, $SU(2)$ and $U(1)$ field strengths. We have assumed CP-conservation. For di-Higgs production allowing also for CP-violating operators see ref. [96]. The effective Lagrangian at dimension-6 can be generally be written in various basis, with the different operators connected by equations of motions. Two different complete basis are the Warsaw basis [95] and the strongly-interacting light Higgs basis (SILH), originally proposed by [97] and completed in [98, 99]. In addition, in [100] the so-called HISZ subset of operators was presented. In the Warsaw basis the effective operators relevant for di-Higgs production are given by

$$\begin{aligned}\Delta \mathcal{L}_{\text{Warsaw}} = & \frac{C_{\phi,\square}}{\Lambda^2} (\phi^\dagger \phi) \square (\phi^\dagger \phi) + \frac{C_{\phi D}}{\Lambda^2} (\phi^\dagger D_\mu \phi)^* (\phi^\dagger D^\mu \phi) + \frac{C_\phi}{\Lambda^2} (\phi^\dagger \phi)^3 \\ & + \left(\frac{C_{u\phi}}{\Lambda^2} \phi^\dagger \phi \bar{q}_L \phi^c t_R + \text{h.c.} \right) + \frac{C_{\phi G}}{\Lambda^2} \phi^\dagger \phi G_{\mu\nu}^a G^{\mu\nu,a} \\ & + \frac{\bar{C}_{uG}}{\Lambda^2} (\bar{q}_L \sigma^{\mu\nu} T^a G_{\mu\nu}^a \tilde{\phi} t_R + \text{h.c.}) ,\end{aligned}\quad (3.3)$$

where $\tilde{\phi}_i = \epsilon_i k \phi_k^*$. While the Warsaw basis is constructed such that derivative operators are systematically removed by equations of motion, two derivative Higgs interactions remain. They contain covariant derivatives rather than simple derivatives and hence cannot be removed by gauge-independent field redefinitions. In order to obtain a canonically normalised Higgs kinetic term the standard field redefinition is

$$H = \begin{pmatrix} 0 \\ h(1 + c_{H,kin}) + v \end{pmatrix} \quad (3.4)$$

with

$$c_{H,kin} = \left(C_{H,\square} - \frac{1}{4} C_{HD} \right) \frac{v^2}{\Lambda^2} . \quad (3.5)$$

This field redefinition though generates derivative Higgs self-interactions, $h(\partial_\mu h)^2$ and $h^2(\partial_\mu h)^2$. For an easier comparison with other effective descriptions which do not appear in the HEFT Lagrangian. Instead one can use a gauge-dependent field redefinition (which

transforms Goldstone/Higgs components in a different way). Such a choice is tricky but we do not need to care for any issues regarding gauge dependence since we do not have gauge fields in the considered process. While the full gauge dependent field redefinition is given for instance in [101], we just need the one of the Higgs

$$h \rightarrow h + c_{H,kin} \left(h + \frac{h^2}{v} + \frac{h^3}{3v^2} \right). \quad (3.6)$$

This field redefinition hence leads to a dependence on $c_{H,kin}$ of all Higgs boson couplings.

The SILH Lagrangian instead can be written as

$$\begin{aligned} \Delta\mathcal{L}_{\text{SILH}} = & \frac{\bar{c}_H}{2v^2} \partial_\mu (\phi^\dagger \phi) \partial^\mu (\phi^\dagger \phi) + \frac{\bar{c}_u}{v^2} y_t (\phi^\dagger \phi \bar{q}_L \tilde{\phi} t_R + \text{h.c.}) - \frac{\bar{c}_6}{2v^2} \frac{m_h^2}{v^2} (\phi^\dagger \phi)^3 \\ & + \frac{\bar{c}_{ug}}{v^2} g_s (\bar{q}_L \sigma^{\mu\nu} G_{\mu\nu} \tilde{\phi} t_R + \text{h.c.}) + \frac{4\bar{c}_g}{v^2} g_s^2 \phi^\dagger \phi G_{\mu\nu}^a G^{a\mu\nu}. \end{aligned} \quad (3.7)$$

A canonical definition of the Higgs kinetic term can be obtained by means of the field redefinition

$$h \rightarrow h - \frac{\bar{c}_H}{2} \left(h + \frac{h^2}{v} + \frac{h^3}{3v^2} \right), \quad (3.8)$$

again leading to a dependence on \bar{c}_H of all Higgs boson couplings. While the operators relevant for di-Higgs production between the SILH and Warsaw basis are basically the same, we have adopted different power counting rules of the coefficients in front of the operators. For eq. (3.3) a purely dimensional power counting was used, while eq. (3.7) reflects the UV prejudice regarding the scaling of the operators, e.g. new physics generating an operator $\phi^\dagger \phi G_{\mu\nu}^a G^{a\mu\nu}$ usually stems from colored new particles that couple with the strong coupling constant to the gluons. In ref. [97] for instance the coefficient in front of this operator contains an extra $1/16\pi^2$ to reflect the loop-suppression of weakly coupled new physics to the effective Higgs gluon coupling.

The relevant terms for di-Higgs production of the HEFT Lagrangian is given by

$$\Delta\mathcal{L}_{\text{HEFT}} = -m_t \left(c_t \frac{h}{v} + c_{tt} \frac{h^2}{v^2} \right) \bar{t} t - c_{hhh} \frac{m_h^2}{2v} h^3 + \frac{\alpha_s}{8\pi} \left(c_{ggh} \frac{h}{v} + c_{gghh} \frac{h^2}{v^2} \right) G_{\mu\nu}^a G^{a,\mu\nu}. \quad (3.9)$$

In contrast to eqs. (3.3) and (3.7) the couplings of one and two Higgs bosons to fermions or gluons become de-correlated. We noted that we have omitted the top quark dipole operator. From the UV point of view of a weakly interacting model such a coupling would enter at the loop level hence effectively have an extra suppression factor of $1/16\pi^2$. In contrast to the $\phi^\dagger \phi G_{\mu\nu}^a G^{a\mu\nu}$ operator that carries such a suppression as well, the dipole-operator enters only via loop diagrams and is hence suppressed compared to all

the other operators assuming a weakly-interacting UV model. In table 3.1 we give the

HEFT	SILH	Warsaw
c_{hhh}	$1 - \frac{3}{2}\bar{c}_H + \bar{c}_6$	$1 - 2\frac{v^4}{m_h^2}C_H + 3c_{H,kin}$
c_t	$1 - \frac{\bar{c}_H}{2} - \bar{c}_u$	$1 + c_{H,kin} - C_{uH}\frac{v^3}{\sqrt{2}m_t}$
c_{tt}	$\frac{-\bar{c}_H + 3\bar{c}_u}{4}$	$-C_{uH}\frac{3v^3}{2\sqrt{2}m_t} + c_{H,kin}$
c_{ggh}	$128\pi^2\bar{c}_g$	$8\pi/\alpha_s v^2 C_{HG}$
c_{gghh}	$64\pi^2\bar{c}_g$	$4\pi/\alpha_s v^2 C_{HG}$

Table 3.1. Leading order translation between different operator basis choices.

translation among the various choices for an effective field theory description. The HEFT is more general than SMEFT allowing for di-Higgs production to vary the couplings of two Higgs bosons to fermions or gluons in an uncorrelated way from the corresponding couplings with a single Higgs boson. While being more general, this obviously also has the disadvantage that more barely constrained couplings enter into di-Higgs production leading potentially to degeneracies in their determination. In table 3.1 we also see that the translation between the Warsaw basis as defined from eq. (??) contains an α_s . Since α_s is a running parameter and for di-Higgs production typically evaluated at $M_{hh}/2$ a translation between the coupling between Warsaw and SILH/HEFT needs to consider this fact. This can be rectified by including the running of C_{HG} at the order at which the running of α_s is considered or by redefining

$$C_{HG} \rightarrow C'_{HG} = \frac{1}{\alpha_s} C_{HG}. \quad (3.10)$$

Finally, we would like to comment on the models which are realised by the different choices for the EFT. Typically, HEFT is the correct choice in strongly-interacting models where the Higgs boson arises as a pseudo-Goldstone boson. Since HEFT does not assume that the Higgs boson transforms within a SM doublet, Goldstone boson scattering is not unitarised by the Higgs boson implying that the HEFT description cannot stay valid for new physics above scales of $\Lambda > 4\pi v$. Generically speaking HEFT assumes larger deviations from the SM. UV models that are generically described by HEFT tend to linearise in the limit in which the coupling deviations are small with respect to the SM. For instance, models like Minimal Composite Higgs Models given the current coupling constraints can in good approximation be described by a linear EFT (SMEFT). Another prime example for HEFT, the dilaton, in its simplest description generically predicts too large coupling deviations in the gluon Higgs couplings [102] and hence also its description via HEFT is challenged. A further example for a UV realisation of HEFT is the singlet model in the strong coupling regime keeping the vacuum expectation value of the singlet

close to the electroweak scale [103?]. The regime where the HEFT should be the preferred description is though where the mixing between singlet and doublet Higgs fields is rather large hence again strongly constrained by single Higgs coupling measurements. In the limit where both the new mass scale, singlet mass and singlet vacuum expectation value, decouple, is well described within SMEFT. A UV dynamics that is described by HEFT and not SMEFT given the current coupling constraints hence remains an open question. Nevertheless, one should keep in mind that HEFT for di-Higgs production is more general and that Higgs pair production is THE place of probing potential de-correlation among couplings of one or two Higgs bosons to fermions or gauge bosons.

Bibliography

- [1] R. A. Minlos, *Introduction to mathematical statistical physics*. No. 19. American Mathematical Soc., 2000.
- [2] M. Gell-Mann, “The eightfold way: A theory of strong interaction symmetry,” <https://www.osti.gov/biblio/4008239>.
- [3] C. N. Yang and R. L. Mills, “Conservation of isotopic spin and isotopic gauge invariance,” *Phys. Rev.* **96** (Oct, 1954) 191–195.
<https://link.aps.org/doi/10.1103/PhysRev.96.191>.
- [4] **Particle Data Group** Collaboration, P. Zyla *et al.*, “Review of Particle Physics,” *PTEP* **2020** no. 8, (2020) 083C01.
- [5] D. S. Freed, “Lectures on topological quantum field theory,” 1993.
- [6] R. Dijkgraaf and E. Witten, “Topological gauge theories and group cohomology,” *Communications in Mathematical Physics* **129** no. 2, (1990) 393–429.
- [7] A. Salam and J. C. Ward, “On a gauge theory of elementary interactions,” *Il Nuovo Cimento (1955-1965)* **19** no. 1, (1961) 165–170.
<https://doi.org/10.1007/BF02812723>.
- [8] A. Salam and J. C. Ward, “Weak and electromagnetic interactions,” *Il Nuovo Cimento (1955-1965)* **11** no. 4, (1959) 568–577.
<https://doi.org/10.1007/BF02726525>.
- [9] S. Weinberg, “A model of leptons,” *Phys. Rev. Lett.* **19** (Nov, 1967) 1264–1266.
<https://link.aps.org/doi/10.1103/PhysRevLett.19.1264>.
- [10] F. Capozzi, E. Lisi, A. Marrone, D. Montanino, and A. Palazzo, “Neutrino masses and mixings: Status of known and unknown 3ν parameters,” *Nucl. Phys. B* **908** (2016) 218–234, [arXiv:1601.07777 \[hep-ph\]](https://arxiv.org/abs/1601.07777).
- [11] **ALEPH, DELPHI, L3, OPAL, SLD, LEP Electroweak Working Group, SLD Electroweak Group, SLD Heavy Flavour Group** Collaboration, S. Schael *et al.*, “Precision electroweak measurements on the Z resonance,” *Phys. Rept.* **427** (2006) 257–454, [arXiv:hep-ex/0509008 \[hep-ex\]](https://arxiv.org/abs/hep-ex/0509008).

Bibliography

- [12] **SLD** Collaboration, K. Abe *et al.*, “First direct measurement of the parity violating coupling of the Z0 to the s quark,” *Phys. Rev. Lett.* **85** (2000) 5059–5063, [arXiv:hep-ex/0006019](https://arxiv.org/abs/hep-ex/0006019).
- [13] **CDF, D0** Collaboration, T. E. W. Group, “2012 Update of the Combination of CDF and D0 Results for the Mass of the W Boson,” [arXiv:1204.0042 \[hep-ex\]](https://arxiv.org/abs/1204.0042).
- [14] **ALEPH, DELPHI, L3, OPAL, LEP Electroweak** Collaboration, S. Schael *et al.*, “Electroweak Measurements in Electron-Positron Collisions at W-Boson-Pair Energies at LEP,” *Phys. Rept.* **532** (2013) 119–244, [arXiv:1302.3415 \[hep-ex\]](https://arxiv.org/abs/1302.3415).
- [15] **DØ** Collaboration, V. M. Abazov *et al.*, “Measurement of $\sin^2 \theta_{\text{eff}}^\ell$ and Z-light quark couplings using the forward-backward charge asymmetry in $p\bar{p} \rightarrow Z/\gamma^* \rightarrow e^+e^-$ events with $\mathcal{L} = 5.0 \text{ fb}^{-1}$ at $\sqrt{s} = 1.96 \text{ TeV}$,” *Phys. Rev. D* **84** (2011) 012007, [arXiv:1104.4590 \[hep-ex\]](https://arxiv.org/abs/1104.4590).
- [16] **CMS** Collaboration, V. Khachatryan *et al.*, “Measurement of the t-channel single-top-quark production cross section and of the $|V_{tb}|$ CKM matrix element in pp collisions at $\sqrt{s}= 8 \text{ TeV}$,” *JHEP* **06** (2014) 090, [arXiv:1403.7366 \[hep-ex\]](https://arxiv.org/abs/1403.7366).
- [17] **ATLAS** Collaboration, M. Aaboud *et al.*, “Measurement of the W -boson mass in pp collisions at $\sqrt{s} = 7 \text{ TeV}$ with the ATLAS detector,” *Eur. Phys. J. C* **78** no. 2, (2018) 110, [arXiv:1701.07240 \[hep-ex\]](https://arxiv.org/abs/1701.07240). [Erratum: Eur.Phys.J.C 78, 898 (2018)].
- [18] Y. Nambu, “Quasi-particles and gauge invariance in the theory of superconductivity,” *Phys. Rev.* **117** (Feb, 1960) 648–663.
<https://link.aps.org/doi/10.1103/PhysRev.117.648>.
- [19] J. Goldstone, “Field theories with superconductor solutions,” *Il Nuovo Cimento (1955-1965)* **19** no. 1, (1961) 154–164.
- [20] J. Goldstone, A. Salam, and S. Weinberg, “Broken symmetries,” *Phys. Rev.* **127** (Aug, 1962) 965–970. <https://link.aps.org/doi/10.1103/PhysRev.127.965>.
- [21] P. W. Anderson, “Plasmons, gauge invariance, and mass,” *Phys. Rev.* **130** (Apr, 1963) 439–442. <https://link.aps.org/doi/10.1103/PhysRev.130.439>.
- [22] F. Englert and R. Brout, “Broken symmetry and the mass of gauge vector mesons,” *Phys. Rev. Lett.* **13** (Aug, 1964) 321–323.
<https://link.aps.org/doi/10.1103/PhysRevLett.13.321>.

- [23] P. W. Higgs, “Broken symmetries and the masses of gauge bosons,” *Phys. Rev. Lett.* **13** (Oct, 1964) 508–509.
<https://link.aps.org/doi/10.1103/PhysRevLett.13.508>.
- [24] G. S. Guralnik, C. R. Hagen, and T. W. B. Kibble, “Global conservation laws and massless particles,” *Phys. Rev. Lett.* **13** (Nov, 1964) 585–587.
<https://link.aps.org/doi/10.1103/PhysRevLett.13.585>.
- [25] G. S. Guralnik, “The History of the Guralnik, Hagen and Kibble development of the Theory of Spontaneous Symmetry Breaking and Gauge Particles,” *Int. J. Mod. Phys. A* **24** (2009) 2601–2627, [arXiv:0907.3466 \[physics.hist-ph\]](https://arxiv.org/abs/0907.3466).
- [26] J. Erler and M. Schott, “Electroweak Precision Tests of the Standard Model after the Discovery of the Higgs Boson,” *Prog. Part. Nucl. Phys.* **106** (2019) 68–119, [arXiv:1902.05142 \[hep-ph\]](https://arxiv.org/abs/1902.05142).
- [27] CMS Collaboration, S. Chatrchyan *et al.*, “Observation of a New Boson at a Mass of 125 GeV with the CMS Experiment at the LHC,” *Phys. Lett. B* **716** (2012) 30–61, [arXiv:1207.7235 \[hep-ex\]](https://arxiv.org/abs/1207.7235).
- [28] ATLAS Collaboration, G. Aad *et al.*, “Observation of a new particle in the search for the Standard Model Higgs boson with the ATLAS detector at the LHC,” *Phys. Lett. B* **716** (2012) 1–29, [arXiv:1207.7214 \[hep-ex\]](https://arxiv.org/abs/1207.7214).
- [29] N. Cabibbo, “Unitary symmetry and leptonic decays,” *Phys. Rev. Lett.* **10** (Jun, 1963) 531–533. <https://link.aps.org/doi/10.1103/PhysRevLett.10.531>.
- [30] M. Kobayashi and T. Maskawa, “CP-Violation in the Renormalizable Theory of Weak Interaction,” *Progress of Theoretical Physics* **49** no. 2, (02, 1973) 652–657, <https://academic.oup.com/ptp/article-pdf/49/2/652/5257692/49-2-652.pdf>.
<https://doi.org/10.1143/PTP.49.652>.
- [31] R. E. Behrends, R. J. Finkelstein, and A. Sirlin, “Radiative corrections to decay processes,” *Phys. Rev.* **101** (Jan, 1956) 866–873.
<https://link.aps.org/doi/10.1103/PhysRev.101.866>.
- [32] T. Kinoshita and A. Sirlin, “Radiative corrections to fermi interactions,” *Phys. Rev.* **113** (Mar, 1959) 1652–1660.
<https://link.aps.org/doi/10.1103/PhysRev.113.1652>.
- [33] I. Mohammad and A. Donnachie, “Radiative Corrections to Radiative Muon Decay.”
- [34] T. van Ritbergen and R. G. Stuart, “Complete 2-loop quantum electrodynamic contributions to the muon lifetime in the fermi model,” *Phys. Rev. Lett.* **82** (Jan, 1999) 488–491. <https://link.aps.org/doi/10.1103/PhysRevLett.82.488>.

Bibliography

- [35] D. Ross and M. Veltman, “Neutral currents and the higgs mechanism,” *Nuclear Physics B* **95** no. 1, (1975) 135–147.
<https://www.sciencedirect.com/science/article/pii/055032137590485X>.
- [36] A. Djouadi, “The Anatomy of electro-weak symmetry breaking. I: The Higgs boson in the standard model,” *Phys. Rept.* **457** (2008) 1–216,
[arXiv:hep-ph/0503172](https://arxiv.org/abs/hep-ph/0503172).
- [37] M. J. Dugan, H. Georgi, and D. B. Kaplan, “Anatomy of a composite higgs model,” *Nuclear Physics* **254** (1985) 299–326.
- [38] C. T. Hill and E. H. Simmons, “Strong Dynamics and Electroweak Symmetry Breaking,” *Phys. Rept.* **381** (2003) 235–402, [arXiv:hep-ph/0203079](https://arxiv.org/abs/hep-ph/0203079). [Erratum: Phys.Rept. 390, 553–554 (2004)].
- [39] M. Schwartz, *Quantum Field Theory and the Standard Model*. Quantum Field Theory and the Standard Model. Cambridge University Press, 2014.
<https://books.google.nl/books?id=HbdEAgAAQBAJ>.
- [40] M. Peskin and D. Schroeder, *An Introduction To Quantum Field Theory*. Frontiers in Physics. Avalon Publishing, 1995.
<https://books.google.de/books?id=EVeNNcslvXOC>.
- [41] M. Einhorn, D. Jones, and M. Veltman, “Heavy particles and the rho parameter in the standard model,” *Nuclear Physics B* **191** no. 1, (1981) 146–172.
<https://www.sciencedirect.com/science/article/pii/0550321381902923>.
- [42] M. E. Peskin and T. Takeuchi, “New constraint on a strongly interacting higgs sector,” *Phys. Rev. Lett.* **65** (Aug, 1990) 964–967.
<https://link.aps.org/doi/10.1103/PhysRevLett.65.964>.
- [43] M. E. Peskin and T. Takeuchi, “Estimation of oblique electroweak corrections,” 1991.
- [44] M. Golden and L. Randall, “Radiative corrections to electroweak parameters in technicolor theories,” *Nuclear Physics B* **361** no. 1, (1991) 3–23.
<https://www.sciencedirect.com/science/article/pii/0550321391906144>.
- [45] B. Holdom and J. Terning, “Large corrections to electroweak parameters in technicolor theories,” *Physics Letters B* **247** no. 1, (1990) 88–92.
<https://www.sciencedirect.com/science/article/pii/037026939091054F>.
- [46] G. Altarelli, R. Barbieri, and S. Jadach, “Toward a model-independent analysis of electroweak data,” *Nuclear Physics B* **369** no. 1, (1992) 3–32.
<https://www.sciencedirect.com/science/article/pii/055032139290376M>.

- [47] R. S. Chivukula, S. B. Selipsky, and E. H. Simmons, “Nonoblique effects in the $b\bar{b}^+$ vertex from extended technicolor dynamics,” *Phys. Rev. Lett.* **69** (Jul, 1992) 575–577. <https://link.aps.org/doi/10.1103/PhysRevLett.69.575>.
- [48] E. H. Simmons, R. S. Chivukula, and J. Terning, “Testing extended technicolor with $R(b)$,” *Prog. Theor. Phys. Suppl.* **123** (1996) 87–96, [arXiv:hep-ph/9509392](https://arxiv.org/abs/hep-ph/9509392).
- [49] G. Valencia and S. Willenbrock, “Goldstone-boson equivalence theorem and the higgs resonance,” *Phys. Rev. D* **42** (Aug, 1990) 853–859. <https://link.aps.org/doi/10.1103/PhysRevD.42.853>.
- [50] L. Di Luzio, R. Gröber, and M. Spannowsky, “Maxi-sizing the trilinear Higgs self-coupling: how large could it be?,” *Eur. Phys. J. C* **77** no. 11, (2017) 788, [arXiv:1704.02311 \[hep-ph\]](https://arxiv.org/abs/1704.02311).
- [51] M. Lindner, “Implications of Triviality for the Standard Model,” *Z. Phys. C* **31** (1986) 295.
- [52] M. Sher, “Electroweak Higgs Potentials and Vacuum Stability,” *Phys. Rept.* **179** (1989) 273–418.
- [53] J. A. Casas, J. R. Espinosa, and M. Quiros, “Standard model stability bounds for new physics within LHC reach,” *Phys. Lett. B* **382** (1996) 374–382, [arXiv:hep-ph/9603227](https://arxiv.org/abs/hep-ph/9603227).
- [54] G. Isidori, G. Ridolfi, and A. Strumia, “On the metastability of the standard model vacuum,” *Nucl. Phys. B* **609** (2001) 387–409, [arXiv:hep-ph/0104016](https://arxiv.org/abs/hep-ph/0104016).
- [55] G. Degrassi, S. Di Vita, J. Elias-Miro, J. R. Espinosa, G. F. Giudice, G. Isidori, and A. Strumia, “Higgs mass and vacuum stability in the Standard Model at NNLO,” *JHEP* **08** (2012) 098, [arXiv:1205.6497 \[hep-ph\]](https://arxiv.org/abs/1205.6497).
- [56] J. Ellis, “Physics goals of the next century@ cern,” in *AIP Conference Proceedings*, vol. 542, pp. 267–292, American Institute of Physics. 2000.
- [57] “LHC-facts.” <http://www.lhc-facts.ch>.
- [58] “Weltmaschine- CERN und LHC.” https://www.weltmaschine.de/cern_und_lhc/lhc/.
- [59] “LHC Design Report Vol.1: The LHC Main Ring.”
- [60] “LHC long term schedule .” <https://lhc-commissioning.web.cern.ch/schedule/LHC-long-term.htm>.

Bibliography

- [61] “High-Luminosity Large Hadron Collider (HL-LHC) : Preliminary Design Report.”
- [62] “LHC preformance tracking.” <https://bpt.web.cern.ch/lhc/>.
- [63] “Taking a look at the LHC.”
https://www.lhc-closer.de/taking_a_closer_look_at_lhc/0.luminosity.
- [64] “ATLAS Run 2 luminosity public results .” <https://twiki.cern.ch/twiki/bin/view/AtlasPublic/LuminosityPublicResults>.
- [65] “CMS luminosity public results .”
<https://twiki.cern.ch/twiki/bin/view/CMSPublic/LumiPublicResults>.
- [66] “ATLAS Run 2 luminosity public results .” <https://twiki.cern.ch/twiki/bin/view/AtlasPublic/LuminosityPublicResultsRun2>.
- [67] S. Fartoukh *et al.*, “LHC Configuration and Operational Scenario for Run 3,” tech. rep., CERN, Geneva, Nov, 2021. <https://cds.cern.ch/record/2790409>.
- [68] **CMS** Collaboration, A. M. Sirunyan *et al.*, “A measurement of the Higgs boson mass in the diphoton decay channel,” *Phys. Lett. B* **805** (2020) 135425, [arXiv:2002.06398 \[hep-ex\]](https://arxiv.org/abs/2002.06398).
- [69] **ATLAS** Collaboration, M. Aaboud *et al.*, “Measurement of the Higgs boson mass in the $H \rightarrow ZZ^* \rightarrow 4\ell$ and $H \rightarrow \gamma\gamma$ channels with $\sqrt{s} = 13$ TeV pp collisions using the ATLAS detector,” *Phys. Lett. B* **784** (2018) 345–366, [arXiv:1806.00242 \[hep-ex\]](https://arxiv.org/abs/1806.00242).
- [70] **ATLAS, CMS** Collaboration, G. Aad *et al.*, “Combined Measurement of the Higgs Boson Mass in pp Collisions at $\sqrt{s} = 7$ and 8 TeV with the ATLAS and CMS Experiments,” *Phys. Rev. Lett.* **114** (2015) 191803, [arXiv:1503.07589 \[hep-ex\]](https://arxiv.org/abs/1503.07589).
- [71] **CMS** Collaboration, A. M. Sirunyan *et al.*, “Measurements of properties of the Higgs boson decaying into the four-lepton final state in pp collisions at $\sqrt{s} = 13$ TeV,” *JHEP* **11** (2017) 047, [arXiv:1706.09936 \[hep-ex\]](https://arxiv.org/abs/1706.09936).
- [72] P. M. Aronow and B. T. Miller, *Foundations of Agnostic Statistics*. Cambridge University Press, 2019.
- [73] J. De Blas, G. Durieux, C. Grojean, J. Gu, and A. Paul, “On the future of Higgs, electroweak and diboson measurements at lepton colliders,” *JHEP* **12** (2019) 117, [arXiv:1907.04311 \[hep-ph\]](https://arxiv.org/abs/1907.04311).

- [74] S. Banerjee, R. S. Gupta, O. Ochoa-Valeriano, and M. Spannowsky, “High energy lepton colliders as the ultimate Higgs microscopes,” [arXiv:2109.14634 \[hep-ph\]](https://arxiv.org/abs/2109.14634).
- [75] **ATLAS** Collaboration, M. Aaboud *et al.*, “Constraints on off-shell Higgs boson production and the Higgs boson total width in $ZZ \rightarrow 4\ell$ and $ZZ \rightarrow 2\ell 2\nu$ final states with the ATLAS detector,” *Phys. Lett. B* **786** (2018) 223–244, [arXiv:1808.01191 \[hep-ex\]](https://arxiv.org/abs/1808.01191).
- [76] **CMS** Collaboration, A. M. Sirunyan *et al.*, “Measurements of the Higgs boson width and anomalous HVV couplings from on-shell and off-shell production in the four-lepton final state,” *Phys. Rev. D* **99** no. 11, (2019) 112003, [arXiv:1901.00174 \[hep-ex\]](https://arxiv.org/abs/1901.00174).
- [77] **ATLAS** Collaboration, G. Aad *et al.*, “Study of the spin and parity of the Higgs boson in diboson decays with the ATLAS detector,” *Eur. Phys. J. C* **75** no. 10, (2015) 476, [arXiv:1506.05669 \[hep-ex\]](https://arxiv.org/abs/1506.05669). [Erratum: Eur.Phys.J.C 76, 152 (2016)].
- [78] **CMS** Collaboration, V. Khachatryan *et al.*, “Constraints on the spin-parity and anomalous HVV couplings of the Higgs boson in proton collisions at 7 and 8 TeV,” *Phys. Rev. D* **92** no. 1, (2015) 012004, [arXiv:1411.3441 \[hep-ex\]](https://arxiv.org/abs/1411.3441).
- [79] **CMS** Collaboration, V. Khachatryan *et al.*, “Measurement of differential and integrated fiducial cross sections for Higgs boson production in the four-lepton decay channel in pp collisions at $\sqrt{s} = 7$ and 8 TeV,” *JHEP* **04** (2016) 005, [arXiv:1512.08377 \[hep-ex\]](https://arxiv.org/abs/1512.08377).
- [80] “Measurements of the total cross sections for Higgs boson production combining the $H \rightarrow \gamma\gamma$ and $H \rightarrow ZZ^* \rightarrow 4\ell$ decay channels at 7, 8 and 13 TeV center-of-mass energies with the ATLAS detector,”.
- [81] **CMS** Collaboration, A. M. Sirunyan *et al.*, “Measurement and interpretation of differential cross sections for Higgs boson production at $\sqrt{s} = 13$ TeV,” *Phys. Lett. B* **792** (2019) 369–396, [arXiv:1812.06504 \[hep-ex\]](https://arxiv.org/abs/1812.06504).
- [82] **CMS** Collaboration, A. M. Sirunyan *et al.*, “Measurements of production cross sections of the Higgs boson in the four-lepton final state in proton–proton collisions at $\sqrt{s} = 13$ TeV,” *Eur. Phys. J. C* **81** no. 6, (2021) 488, [arXiv:2103.04956 \[hep-ex\]](https://arxiv.org/abs/2103.04956).
- [83] **ATLAS** Collaboration, “Combined measurement of the total and differential cross sections in the $H \rightarrow \gamma\gamma$ and the $H \rightarrow ZZ^* \rightarrow 4\ell$ decay channels at $\sqrt{s} = 13$ TeV with the ATLAS detector,”.

Bibliography

- [84] **ATLAS** Collaboration, “Measurements and interpretations of Higgs-boson fiducial cross sections in the diphoton decay channel using 139 fb^{-1} of pp collision data at $\sqrt{s} = 13 \text{ TeV}$ with the ATLAS detector,”.
- [85] **CMS** Collaboration, “Measurements of properties of the Higgs boson in the four-lepton final state in proton-proton collisions at $\sqrt{s} = 13 \text{ TeV}$,”.
- [86] N. Berger *et al.*, “Simplified Template Cross Sections - Stage 1.1,” [arXiv:1906.02754 \[hep-ph\]](https://arxiv.org/abs/1906.02754).
- [87] **ATLAS** Collaboration, “A combination of measurements of Higgs boson production and decay using up to 139 fb^{-1} of proton–proton collision data at $\sqrt{s} = 13 \text{ TeV}$ collected with the ATLAS experiment,” Tech. Rep. ATLAS-CONF-2020-027, 2020.
- [88] **CMS** Collaboration, A. M. Sirunyan *et al.*, “Measurements of Higgs boson production cross sections and couplings in the diphoton decay channel at $\sqrt{s} = 13 \text{ TeV}$,” *JHEP* **07** (2021) 027, [arXiv:2103.06956 \[hep-ex\]](https://arxiv.org/abs/2103.06956).
- [89] **CMS Collaboration** Collaboration, “Sensitivity projections for Higgs boson properties measurements at the HL-LHC,” tech. rep., CERN, Geneva, 2018. <https://cds.cern.ch/record/2647699>.
- [90] **CMS** Collaboration, “Combined Higgs boson production and decay measurements with up to 137 fb^{-1} of proton-proton collision data at $\text{sqrt}s = 13 \text{ TeV}$,” Tech. Rep. CMS-PAS-HIG-19-005, 2020.
- [91] **CMS** Collaboration, “Measurement of Higgs boson production in association with a W or Z boson in the $H \rightarrow WW$ decay channel,” Tech. Rep. CMS-PAS-HIG-19-017, 2021.
- [92] **ATLAS** Collaboration, “Combined measurements of Higgs boson production and decay using up to 139 fb^{-1} of proton-proton collision data at $\sqrt{s} = 13 \text{ TeV}$ collected with the ATLAS experiment,”.
- [93]
- [94] **CMS** Collaboration, A. M. Sirunyan *et al.*, “Search for associated production of a Higgs boson and a single top quark in proton-proton collisions at $\sqrt{s} = 13 \text{ TeV}$,” *Phys. Rev. D* **99** no. 9, (2019) 092005, [arXiv:1811.09696 \[hep-ex\]](https://arxiv.org/abs/1811.09696).
- [95] B. Grzadkowski, M. Iskrzynski, M. Misiak, and J. Rosiek, “Dimension-Six Terms in the Standard Model Lagrangian,” *JHEP* **10** (2010) 085, [arXiv:1008.4884 \[hep-ph\]](https://arxiv.org/abs/1008.4884).

- [96] R. Grober, M. Muhlleitner, and M. Spira, “Higgs Pair Production at NLO QCD for CP-violating Higgs Sectors,” *Nucl. Phys. B* **925** (2017) 1–27, [arXiv:1705.05314 \[hep-ph\]](https://arxiv.org/abs/1705.05314).
- [97] G. F. Giudice, C. Grojean, A. Pomarol, and R. Rattazzi, “The Strongly-Interacting Light Higgs,” *JHEP* **06** (2007) 045, [arXiv:hep-ph/0703164](https://arxiv.org/abs/hep-ph/0703164).
- [98] R. Contino, M. Ghezzi, C. Grojean, M. Muhlleitner, and M. Spira, “Effective Lagrangian for a light Higgs-like scalar,” *JHEP* **07** (2013) 035, [arXiv:1303.3876 \[hep-ph\]](https://arxiv.org/abs/1303.3876).
- [99] J. Elias-Miró, C. Grojean, R. S. Gupta, and D. Marzocca, “Scaling and tuning of EW and Higgs observables,” *JHEP* **05** (2014) 019, [arXiv:1312.2928 \[hep-ph\]](https://arxiv.org/abs/1312.2928).
- [100] K. Hagiwara, S. Ishihara, R. Szalapski, and D. Zeppenfeld, “Low-energy effects of new interactions in the electroweak boson sector,” *Phys. Rev. D* **48** (1993) 2182–2203.
- [101] C. Hartmann and M. Trott, “Higgs Decay to Two Photons at One Loop in the Standard Model Effective Field Theory,” *Phys. Rev. Lett.* **115** no. 19, (2015) 191801, [arXiv:1507.03568 \[hep-ph\]](https://arxiv.org/abs/1507.03568).
- [102] B. Bellazzini, C. Csaki, J. Hubisz, J. Serra, and J. Terning, “A Higgslike Dilaton,” *Eur. Phys. J. C* **73** no. 2, (2013) 2333, [arXiv:1209.3299 \[hep-ph\]](https://arxiv.org/abs/1209.3299).
- [103] G. Buchalla, O. Cata, A. Celis, and C. Krause, “Standard Model Extended by a Heavy Singlet: Linear vs. Nonlinear EFT,” *Nucl. Phys. B* **917** (2017) 209–233, [arXiv:1608.03564 \[hep-ph\]](https://arxiv.org/abs/1608.03564).